Journal of Statistical Physics, Vol. 58, Nos. 1/2, 1990

Discrete Network Models for the Low-Field Hall Effect near a Percolation Threshold: Theory and Simulations

David J. Bergman,[1,2] Edgardo Duering,[3,4] and Michael Murat[3,5]

Received April 7, 1989; revision received August 14, 1989

The critical behavior of the weak-field Hall effect near a percolation threshold is studied with the help of two discrete random network models. Many finite realizations of such networks at the percolation threshold are produced and solved to yield the potentials at all sites. A new algorithm for doing that was developed that is based on the transfer matrix method. The site potentials are used to calculate the bulk effective Hall conductivity and Hall coefficient, as well as some other properties, such as the Ohmic conductivity, the size of the backbone, and the number of binodes. Scaling behavior for these quantities as power laws of the network size is determined and values of the critical exponents are found.

KEY WORDS: Hall effect; percolation; network models; transfer matrix algorithm; duality.

1. INTRODUCTION

Interest in the critical behavior of the Hall effect near a metal–insulator transition of the percolative type developed rather slowly after the early, pioneering theoretical work of Juretschke *et al.*[1] This gradual develop-

[1] Permanent address: School of Physics and Astronomy, Raymond and Beverly Sackler Faculty of Exact Sciences, Tel Aviv University, Tel Aviv 69978, Israel.
[2] Department of Physics, Ohio State University, Columbus, Ohio 43210-1106.
[3] School of Physics and Astronomy, Raymond and Beverly Sackler Faculty of Exact Sciences, Tel Aviv University, Tel Aviv 69978, Israel.
[4] Present address: Department of Chemical Physics, Weizmann Institute of Science, Rehovoth, Israel.
[5] Present address: Science Laboratories, Exxon Research and Engineering, Annandale, New Jersey 08801.

0022-4715/90/0100-0001$06.00/0

ment included an effective medium theory,[2] early attempts at simulations of random network models,[3] a links–nodes picture of the Hall effect,[4] and exact treatments of a Cayley-tree network[5] and of two-dimensional systems.[1] It has culminated in recent years in the development of a full-fledged scaling theory for the critical behavior of the Hall effect near the percolation threshold p_c,[6] and the discovery of a reliable network model and of an efficient method for calculating the Hall conductivity from simulations of this model.[7] Preliminary values calculated in this way for the critical exponents,[8] as well as some predictions of the scaling theory,[6] have recently been dramatically verified in two beautiful experiments.[9,10]

In this article we describe detailed calculations that have been performed to simulate the low-field Hall effect at the percolation threshold in randomly diluted network models of finite size L. Two different models were used—we started out with the model of ref. 7, but in the course of the work we discovered a new model, which is better in some respects. Results from both models will be presented. The method used to calculate the Hall conductivity required us to find the detailed current distribution on all the current-carrying bonds of the network. We developed a new method for doing this which is based on the transfer matrix approach of Derrida and Vannimenus.[11] The current distributions produced by this method can also be used for detailed investigations of the statistical properties of these distributions and their various moments.[12] The method, which is more precise than relaxation calculations and much more efficient than a direct solution of Kirchhoff's equations by matrix inversion, is described in detail here for the first time. The calculations reported here were performed entirely on samples of cubic shape $L \times L \times L$. The scaling behavior as a power of L was determined from these simulations for the bulk effective Ohmic and Hall conductivities σ_e and λ_e, as well as for the bulk effective Hall coefficient $R_e \equiv \lambda_e/(H\sigma_e^2)$. Using known values for the correlation length exponent ν, we then obtained values for the Ohmic exponent t and for the Hall exponents τ and g,

$$\begin{aligned} \sigma_e &\sim \Delta p^t \\ \lambda_e &\sim \Delta p^\tau \\ R_e &\sim \Delta p^{-g} \end{aligned} \tag{1.1}$$

where

$$\Delta p \equiv p - p_c, \qquad g = 2t - \tau$$

From our simulations we also determined two geometrical quantities, the size N_B of the percolating backbone at p_c, and the density of binodes

N_{BN} in the model of ref. 7: In that model each sample consists of four electrically unconnected networks that nevertheless intersect each other. The points of intersection between two backbones are called binodes. For these two numbers we also found an asymptotic power law dependence on L which is characterized by exponents which have the significance of fractal dimensions

$$N_B \sim L^{D_B}, \qquad N_{BN} \sim L^{D_{BN}} \tag{1.2}$$

The remainder of this article is organized as follows.

In Section 2, we review the theory of the low-field Hall effect in macroscopically inhomogeneous conductors and describe the two discrete network models that we used in order to simulate such a medium near a percolation threshold. In Section 3, we describe our transfer matrix algorithm for calculating the detailed current distribution in a random-resistor network. In Section 4, we present the results of our simulations and the values obtained for the critical exponents t, τ, g, D_B, and D_{BN}. In Section 5, we discuss the significance of these results, compare them to other calculations, and indicate possible directions for future research.

2. THE BASIC CONTINUUM THEORY AND THE DISCRETE MODELS

The Hall effect in a homogeneous continuum conductor appears as an antisymmetric part of the conductivity tensor. The Hall current density can thus be represented as a vector product $\lambda \times \mathbf{E}$, where $\mathbf{E} = -\nabla\phi$ is the electric field and $|\lambda|$ is the local Hall conductivity. For a conductor in which the conductivity tensor is isotropic in zero magnetic field $\mathbf{H} = 0$, λ is parallel to $\mathbf{H}$. When H is small enough, λ is simply proportional to $\mathbf{H}$ and the ohmic conductivity σ is a scalar, where "small enough" means $|\lambda| \ll \sigma$. The total current density at any point of the composite medium is then given by

$$\mathbf{J}(\mathbf{r}) = \sigma(\mathbf{r})\,\mathbf{E}(\mathbf{r}) - \lambda(\mathbf{r}) \times \mathbf{E}(\mathbf{r}) \tag{2.1}$$

where both $\sigma(\mathbf{r})$ and the magnitude and sign (but not the direction) of $\lambda(\mathbf{r})$ have a fixed (but different) value in each component. The direction of $\lambda(\mathbf{r})$ is always either parallel or antiparallel to $\mathbf{H}$. Although both σ and λ have a simple dependence on H when $\lambda \ll \sigma$, namely, $\sigma \sim H^0$ and $\lambda \sim H^1$, if we try to analyze the H dependence of J we must not forget that the electric field E now also depends on H. We can write E as an expansion in powers of H, keeping terms up to order H^1,

$$\begin{aligned} &\mathbf{E} = \mathbf{E}_0 + \mathbf{E}_1 + \cdots \\ &E_0 \sim H^0, \qquad E_1 \sim H^1, \qquad \text{etc.} \end{aligned} \tag{2.2}$$

The bulk effective conductivities $\ddot{\sigma}_e$ and λ_e of the composite conductor are defined by writing an expression like (2.1) for the volume averages of J and E,

$$\langle \mathbf{J} \rangle = \ddot{\sigma}_e \langle \mathbf{E} \rangle - \lambda_e \times \langle \mathbf{E} \rangle \tag{2.3}$$

where the Ohmic conductivity $\ddot{\sigma}_e$ is, in general, a symmetric tensor independent of H, while the Hall conductivity λ_e is a vector that is linear and homogeneous in the components of H but may point in a different direction. When the boundary conditions are such that the electric field would be uniform (and consequently also independent of H), $\mathbf{E}(\mathbf{r}) \equiv \mathbf{E}_{00}(\mathbf{r})$ if the medium were homogeneous, it is not difficult to show that (see Appendix A)

$$\begin{aligned} \langle \mathbf{E} \rangle &= \langle \mathbf{E}_0 \rangle = \mathbf{E}_{00} \\ \langle \mathbf{E}_1 \rangle &= \langle \mathbf{E}_2 \rangle = \cdots = 0 \end{aligned} \tag{2.4}$$

Substituting (2.1) in (2.3) and expanding both sides in powers of H, it is then possible to obtain the following expressions for $\ddot{\sigma}_e$ and λ_e (this is shown for a special case in ref. 7, while a general derivation appears in Appendix A of the present article)

$$\begin{aligned} \mathbf{E}_{00}^{(e)} \cdot \ddot{\sigma}_e \cdot \mathbf{E}_{00}^{(f)} &= \frac{1}{V} \int dV \, \sigma(\mathbf{r}) \, \mathbf{E}_0^{(e)}(\mathbf{r}) \cdot \mathbf{E}_0^{(f)}(\mathbf{r}) \\ &= \frac{1}{V} \int dV \, \sigma(\mathbf{r}) \, \mathbf{E}_0^{(e)}(\mathbf{r}) \cdot \mathbf{E}_{00}^{(f)} \end{aligned} \tag{2.5}$$

$$\lambda_e \cdot (\mathbf{E}_{00}^{(e)} \times \mathbf{E}_{00}^{(f)}) = \frac{1}{V} \int dV \, \lambda(\mathbf{r}) \cdot [\mathbf{E}_0^{(e)}(\mathbf{r}) \times \mathbf{E}_0^{(f)}(\mathbf{r})] \tag{2.6}$$

The upper index which appears in the electric fields here refers to the boundary conditions: $\mathbf{E}_0^{(e)}(\mathbf{r})$ is calculated for boundary conditions such that the average or uniform field $\mathbf{E}_{00}^{(e)}$ is in the direction of the unit vector $\mathbf{e}$. In fact, for convenience we will usually normalize these boundary conditions so that $\mathbf{E}_{00}^{(e)} = \mathbf{e}$. While (2.5) is a standard expression, an expression like (2.6) first appeared in ref. 7. We note that in order to use (2.6), there is no need to calculate any corrections to E_0 due to the presence of a nonzero H—all we need is to calculate $\mathbf{E}_0(\mathbf{r})$ (i.e., at $H = 0$) in the same material for two different sets of boundary conditions, e.g., such that the average field $\mathbf{E}_{00}$ is in the x and y directions.

One can eliminate the subvolume of one of the components from the integration in both (2.5) and (2.6). In the case of a two-component com-

posite with either isotropic or cubic point symmetry these expressions can then be simplified to (see Appendix A)

$$\frac{\sigma_e - \sigma_2}{\sigma_1 - \sigma_2} = \frac{1}{V}\int_{r\in\sigma_1} dV[\mathbf{E}_0^{(x)}(\mathbf{r})\cdot\mathbf{e}_x] \tag{2.7}$$

$$\frac{\lambda_e - \lambda_2}{\lambda_1 - \lambda_2} = \frac{1}{V}\int_{r\in\sigma_1} dV(\mathbf{E}_0^{(x)}\times\mathbf{E}_0^{(y)})_z \tag{2.8}$$

where we have taken $\mathbf{E}_{00}^{(x)} = \mathbf{e}_x$ and $\mathbf{E}_{00}^{(y)} = \mathbf{e}_y$, i.e., unit vectors along two coordinate axes. We note that the right-hand side (rhs) of (2.8) is independent of the Hall conductivities.

In the special case of a two-dimensional (2D), two-component composite with H perpendicular to the plane of the sample, the rhs of (2.8) can be calculated explicitly in terms of σ_e,

$$\frac{\lambda_e - \lambda_2}{\lambda_1 - \lambda_2} = \frac{\sigma_e^2 - \sigma_2^2}{\sigma_1^2 - \sigma_2^2} \qquad \text{in 2D} \tag{2.9}$$

This result is obtained by using the duality transformation which in a 2D system relates the local field $\mathbf{E}_0(\mathbf{r})$ of the original problem to the local field in another problem, in which the full local conductivity tensor is replaced everywhere by its inverse (see Appendix C). Among other things, (2.9) enables us to derive the critical behavior of λ_e near a percolation threshold from that of σ_e, as had already been done using other means.[4] Thus, when component 2 is a perfect insulator, $\sigma_2 = \lambda_2 = 0$, (2.9) entails

$$\frac{\lambda_e}{\lambda_1} = \left(\frac{\sigma_e}{\sigma_1}\right)^2 \sim (p_1 - p_c)^{2t} \qquad \text{in 2D} \tag{2.10}$$

when the volume fraction p_1 of the conducting component is above but close to the percolation threshold p_c.

More generally, including 2D as well as 3D metal–insulator composites, we expect to find

$$\frac{\lambda_e}{\lambda_1} \sim (p_1 - p_c)^{\tau} \qquad \text{for} \quad p_1 > p_c \tag{2.11}$$

The Hall coefficient R is given at low fields by

$$R = \lambda/(H\sigma^2) \tag{2.12}$$

and consequently we expect to find in the same regime

$$\frac{R_e}{R_1} \sim (p_1 - p_c)^{-g}, \qquad g \equiv 2t - \tau \tag{2.13}$$

From (2.10) we see that $g = 0$ (R_e remains finite) in 2D. Early simulations of three-dimensional (3D) percolating systems[8] as well as the links–nodes picture[4] indicated that g is between 0.3 and 0.5, i.e., R_e diverges. This is also supported by preliminary experiments.[9,10]

The discussion of critical behavior can be extended to values of p_1 below p_c if component 2 is a poor conductor (i.e., $\sigma_2 \ll \sigma_1$ and $\lambda_2 \ll \lambda_1$) rather than a perfect insulator. A scaling theory was constructed to describe this situation,[6] and one result of that theory is that when $\Delta p \equiv p_c - p_1$ is sufficiently small, the good conductor will dominate the Hall effect even below p_c. Specifically, if

$$\frac{R_1}{R_2} \equiv \frac{\lambda_1}{\lambda_2}\left(\frac{\sigma_2}{\sigma_1}\right)^2 > \Delta p^{2s+g} \tag{2.14}$$

then the Hall coefficient of the composite below p_c should have the same critical behavior as given by (2.13) above p_c, though possibly with a different proportionality coefficient. This prediction is tested in some of our simulations described in Section 4, and used to accumulate better statistics for evaluating the critical exponent g in one of the models.

In order to calculate λ_e for a 3D composite, one needs to know the two fields $\mathbf{E}_0^{(x)}$ and $\mathbf{E}_0^{(y)}$. For a disordered continuum composite medium near a percolation threshold this is an impossible task. The traditional approach has therefore been to approximate such a medium by a percolating discrete network model, counting upon universality to ensure that the critical exponents, at least, will not be affected. If we try to discretize a continuum system by laying upon it a regular grid of sites and bonds, it is quite natural to assign a potential to each site and a current to each bond. The Ohmic portion of the current I_a through a bond a, corresponding to the first term of (2.1), is then naturally given by the product $g_a V_a$, where V_a is the voltage (potential difference) across a and g_a is its conductance. To calculate the Hall portion of this discretized current, corresponding to the second term of (2.1), we first need to discretize the components of $\mathbf{E}$ that are perpendicular to a. This can only be done by using the voltages $V_{\tilde{a}}$ across other bonds $\tilde{a}$ that are perpendicular to a. We thus arrive at the following ansatz as the discretized version of (2.1):

$$I_a = g_a V_a - \sum_{\tilde{a} \in a} \lambda_{a\tilde{a}} V_{\tilde{a}}(\mathbf{e}_H, \tilde{\mathbf{a}}, \mathbf{a}) \tag{2.15}$$

where the sum is over a set of bonds $\tilde{a}$ that are close to a in some sense, and where the triple scalar product of unit vectors along H, $\tilde{a}$, a ensures the proper dependence on the directions of the fields. The precise dependence of the Hall conductance parameter $\lambda_{a\tilde{a}}$ on the bond pair a, $\tilde{a}$ may be chosen

in different ways, and different choices may lead to different types of discrete models for the Hall effect.

The choice of a network model that is appropriate for the Hall effect has turned out to be rather tricky, in contrast to the ease with which such models have been constructed for representing the Ohmic conductivity. In particular, the model used in ref. 3, which allows a Hall current to flow in a conducting bond as a result of a nonzero field which appears across a neighboring perpendicular bond even when that bond is an insulator, leads to incorrect behavior even in the 2D case, where we should get the exact result of (2.9).[8] This failure could be traced to the fact that the random-resistor networks that implemented that model in 2D were not self-dual, in contrast with continuum 2D systems, which are always self-dual (i.e., their microgeometry does not change under the duality transformation). To avoid these problems, a class of models was introduced where the basic element is either a pair (in 2D) or triplet (in 3D) of identical mutually perpendicular bonds, which represent electrically unconnected Ohmic conductors when $H=0$ (see Fig. 1).[7] When $H\neq 0$ a Hall current can flow in each of these bonds as a result of a nonzero voltage on one of the others,

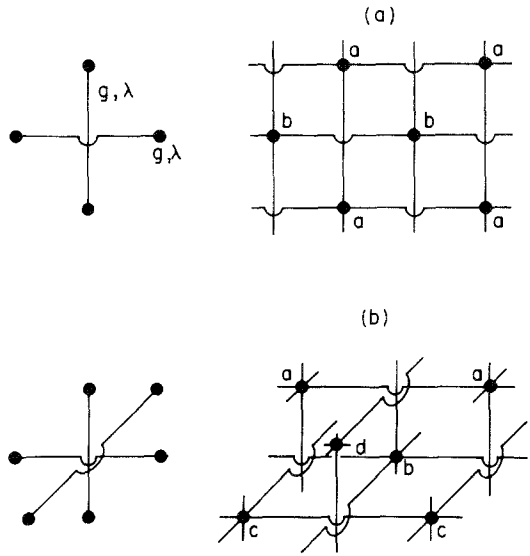

Fig. 1. (a) The basic unit element of two identical, perpendicular, and electrically unconnected conductors and the square-centered, self-dual, 2D network constructed from it. The electrical connections or nodes are marked by black circles. The nodes marked *a* and the nodes marked *b* form two unconnected, but strongly correlated, simple-square, random-bond networks. (b) The basic unit element of three identical, perpendicular, and unconnected conductors and the fcc 3D network constructed from it. The nodes marked *a–d* form four electrically unconnected, correlated, simple-cubic, random-bond networks.

when H has a component that is perpendicular to both bonds. We will call these the class 1 models. When 2D random networks were constructed from these elements they had the expected behavior, including being self-dual. The more interesting 3D case requires simulations of large-scale networks where the voltages on all the bonds must be calculated. In the following section we describe a new method that was developed for doing that.

The class 1 models have one glaring unphysical aspect—they always result in networks that split up into two or more unconnected pieces that occupy the same region of space.[7,8] This is especially annoying in the case of diluted networks just above the percolation threshold. In that case, each of these unconnected networks has its own percolating cluster and backbone, consisting of nodes, links, and blobs, and these govern the Ohmic behavior when $H=0$. When $H\neq 0$, contributions to the macroscopic Hall effect come only from locations where bonds from different, unconnected backbones intersect without making electrical contact—by belonging to the same basic element. These backbone crossings, which we shall call binodes, occur at random locations which are not necessarily near the nodes, and they have no analogue in a real percolating continuum system.

In order to avoid this unphysical feature, we now introduce a new class of models, called class 2, which is a variant of the unacceptable model of ref. 3. In this variant we take a single connected network of the simple square or cubic type and define the electric field in a direction $\tilde{a}$ perpendicular to a given bond a to be a weighted average over the voltages on the four bonds in direction $\tilde{a}$ that are nearest neighbors to a (see Fig. 2). The weight of each of these bonds is 1/4 if it is of the same type as a and

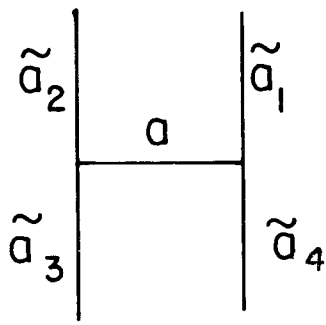

Fig. 2. Planar section of a simple square or simple cubic network showing all the bonds $\tilde{a}_i$ that determine the component of the electric field $E_{a\perp}$ that is in the plane and perpendicular to the bond a. In the model of ref. 3, $E_{a\perp}$ is the simple arithmetic average of all four $V_{\tilde{a}}$'s. In our class 2 models, $E_{a\perp}$ is the weighted average of these $V_{\tilde{a}}$'s, where the weight is 1/4 if the bond $\tilde{a}_i$ is of the same type as a and 0 otherwise.

0 otherwise. In this class of models an electric field in one component cannot produce a Hall current in another component, thus correcting a major flaw in the model of ref. 3. They also avoid the unphysical appearance of binodes which are so crucial in the class 1 models. Moreover, even though the class 2 networks are usually not self-dual in their 2D implementations, the important equality (2.9) can be shown to hold exactly in the weak-field case for such networks of arbitrary size and structure (see Appendix C). We conclude that this is an acceptable model for representing the weak-field Hall effect in 2D, and we can expect it to be a good model to use also in 3D simulations.

The simulations were performed on random-resistor-network models of both classes 1 and 2. The technique in both cases was to find the detailed voltage distribution on all the bonds of the percolating backbones when $H=0$, and then use the discrete analogue of (2.8) in order to find $(\lambda_e-\lambda_2)/(\lambda_1-\lambda_2)$ for $\sigma_2 \ll \sigma_1$. The derivation of the necessary formulas was done in ref. 7 for the class 1 models. In Appendix B this is reviewed and generalized to apply also to the class 2 models. In the following section, we describe the novel algorithm that we developed in order to calculate the voltages on all the current-carrying bonds of the network.

3. NEW METHODS FOR CALCULATING ALL THE BOND VOLTAGES IN A RANDOM-RESISTOR NETWORK

Calculation of the bulk effective Hall conductivity λ_e using the discrete network analogue of (2.8) [see (B.16)] requires knowledge of the voltages on each bond belonging to one of the components—we will always choose this to be the good conductor. This necessitates solution of Kirchhoff's equations for the network. A simple and commonly used method to achieve this goal is to find the site potentials V_k that satisfy

$$V_k = \frac{\sum_a g_a (V_{k+a} - V_k)}{\sum_a g_a} \tag{3.1}$$

using relaxation[13] or sparse matrix inversion[14] techniques. Here a are the lattice vectors from each lattice point to its nearest neighbors, and g_a is the conductance of the bond a. These methods suffer from various problems: Although the computer programs needed are quite simple, the convergence can be very slow, especially when the lattice is close to the percolation threshold of the conducting bonds. One also has to first identify and eliminate all the isolated clusters of conducting bonds, since the potential of such a cluster is undefined. Furthermore, much computer memory is needed, particularly for the inversion method: For a network with n sites one needs to store and invert a matrix of size $n \times n$.

An alternative approach for finding the total conductance is the node elimination method,[15,16] in which one first eliminates the dangling ends and isolated clusters of conducting bonds. One then transforms the network into a simpler one using the star–triangle and other, similar transformations. The method is highly sophisticated and time consuming. It is not immediately clear whether this approach can be usefully extended to an evaluation of all the relevant site potentials.

In the course of the present study, we have developed a new method for the calculation of the site potentials. This is based upon the transfer matrix method,[11,17] which has previously been used successfully for the calculation of the conductance of a network without solving for the site potentials. We will first briefly review the transfer matrix method and then describe the modification which allows an accurate calculation of the site potentials.

Assume that we have a network of resistors as shown in Fig. 3a. Each bond may have an arbitrary (including zero) conductance. If each of the right-hand sites is connected to an external voltage, then due to the linearity of Kirchhoff's equations, we expect a linear dependence of the currents I_i on the voltages V_i. This dependence can be expressed using an *admittance matrix* A as

$$I_i = \sum_j A_{ij} V_j \tag{3.2}$$

Addition of another layer of resistors changes the matrix A to A', which can be calculated exactly and quite simply. The conductance G of the strip between the two equipotential plates is found by setting all $I_k = 0$ $(k \neq 1)$ and calculating the ratio I_1/V_1. In practice, the easiest way of doing this is to add one more layer of zero conductors at the end of the strip.

If the resistors are chosen from a random distribution, the conductance per unit length G/L_z of a strip with L_z layers obviously fluctuates for small L_z, but approaches a limiting value for large enough L_z ($L_z \gg \xi$, where ξ is the correlation length of the random network). Thus, an important advantage of this method over other methods is that one achieves a natural *self-averaging* by building longer strips, without having to worry about which quantity to average (conductance, resistance, or any function of either).

Although this method allows an exact calculation of the conductance of a network without having to identify and eliminate the isolated clusters or dangling ends of conducting bonds, it does not yield the site potentials. However, a simple modification of the method enables us to calculate those, too.

In order to calculate the site potentials at the nth layer (perpendicular to the z direction), we build the network, starting from both ends and

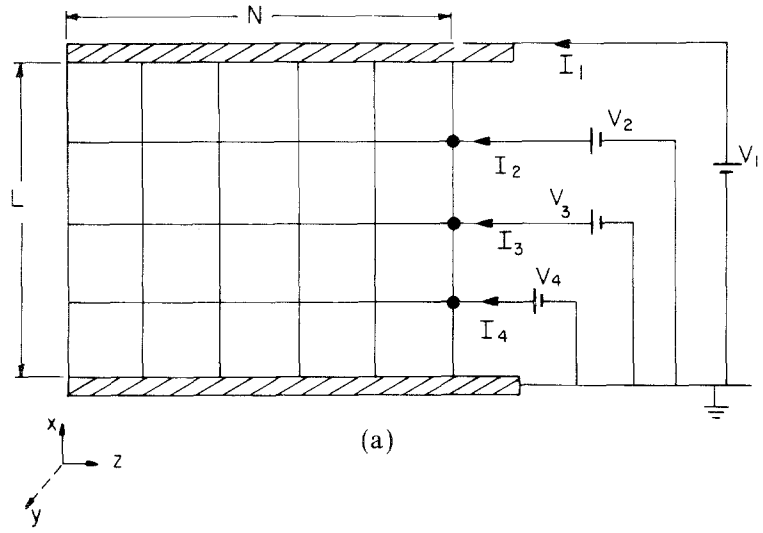

(a)

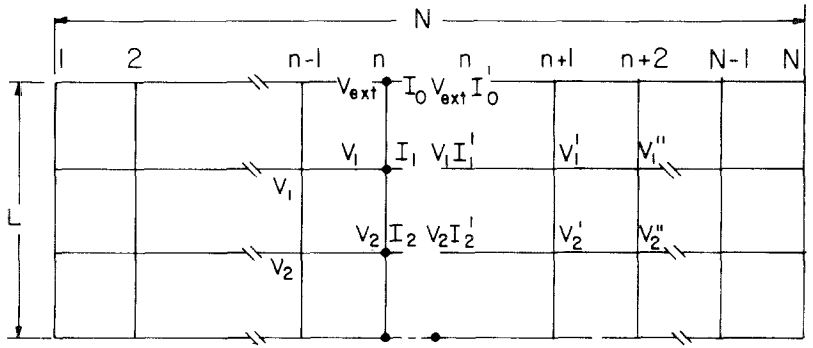

(b)

Fig. 3. (a) A 2D strip network of width $L_x = 4$ and length $L_z = 6$ in the x, z plane. The external voltage is applied between the upper and lower edges of the strip. The relation between the external voltages V_i and the currents I_i is given by (3.2). A 3D strip network is treated in the same way by adding another dimension L_y perpendicular to the plane of the figure. (b) A 2D strip network that is split up at the nth layer into a left subnetwork, built up starting from the left edge and characterized by an admittance matrix A ($I_i = \sum_j A_{ij} V_j$), and a right subnetwork, built up starting from the right edge and characterized by an admittance matrix B ($I_i' = \sum_j B_{ij} V_j$). The sum of currents flowing into corresponding terminals of the two subnetworks must vanish, $I_i + I_i' = 0$ for $i \neq 0$, but $I_0 + I_0' = I_{\text{ext}}$.

ending up at that layer, in the manner described previously. The two subnetworks thus have the sites of the nth layer in common. The admittance matrices for the left and right subnetworks will be denoted by A and B, and the currents entering them by I_k and I'_k, respectively (see Fig. 3b). Since no external current flows into the internal sites, we can write $I_k + I'_k = 0$ for all $k \neq 0$, while $I_0 + I'_0 = I_{\text{ext}}$. In this way we get a set of equations

$$\sum_l (A_{kl} + B_{kl})\, V_l = I_{\text{ext}} \delta_{k0} \tag{3.3}$$

which can be solved numerically to yield all the site potentials in that layer, as well as the total voltage across the network V_0, in terms of the external current I_{ext}. In practice, what we did was to omit from (3.3) the equation for $k = 0$, and assume $V_0\,(= V_{\text{ext}}) = 1$. We then solved the more limited set of equations

$$\sum_{l \neq 0} (A_{kl} + B_{kl})\, V_l = -A_{k0} - B_{k0} \qquad \text{for} \quad k \neq 0 \tag{3.4}$$

in order to determine the remaining V_k.

In the case that the bad conductor is a perfect insulator, we should remove all the isolated clusters from the network before attempting to invert the matrix $A + B$, since the potentials on those clusters are indeterminate. This can be done by first building up the entire network with the same set of random numbers and identifying the sites that are connected to at least one of the external plates by using the Hoshen–Kopelman[18] algorithm. This information is kept on a separate file and used while solving (3.4).

Another way to calculate the V_k of the nth layer is to use only one of the admittance matrices at the nth layer, say A of the left subnetwork, together with the voltages calculated for the next layer to the right, $n + 1$. We must now solve the equation

$$\sum_l A_{kl} V_l = g_k (V'_k - V_k) \tag{3.5}$$

where V'_k is the voltage at the site k of layer $n + 1$. The rhs of this equation is the current I_k entering the kth site from the right subnetwork.

Whereas both of the methods described above lead to good (and also identical) results, the following method does not: When one knows the site voltages on layers $n + 1$ and $n + 2$, V'_k and V''_k, respectively, one could calculate explicitly the current I'_k flowing out of the site k of the right subnetwork. Equating that to the rhs of (3.5), one would then be able to solve for V_k. This procedure is the discrete network equivalent of solving

Laplace's equation with initial conditions on the potential, as well as on its normal derivative. As such, it is well known to be unstable: Any small deviation from the exact solution is quickly amplified and one rapidly attains values of the potential that diverge exponentially fast with distance along the z direction of the strip. (In mathematical jargon, Cauchy's problem with Laplace's equation is "ill-posed.") By contrast, (3.5) is the discrete analogue of a first-order linear differential equation for the potentials V_k as functions of z. Since A is a nonnegative matrix, the equation has no runaway increasing solutions that can lead to amplification of small errors. Therefore, the solutions of (3.5) for V_k can be expected to be stable with small and well-controlled numerical errors. These expectations have all been verified in simulations.

It would require too much machine time to calculate the matrices A and B anew every time we moved to a new layer. We therefore calculate and store the matrices A from all the layers on a permanent file while building up the network in one direction. We then read them backward from the file when the network is being solved in the opposite direction using either (3.4) or (3.5). For a network of cubic shape (i.e., $L_x = L_y = L_z$) this method works very well. However, if we wanted to implement the algorithm for a long strip network in which $L_x \approx L_y \ll L_z$, this would require too much memory. We could then compromise between time and memory limitations by storing the matrices A only for every mth layer. We would thus divide the strip into N/m blocks, in each of which we know the A matrix at the first layer. In order to calculate the potentials within each block, we would read the A matrix of the first layer and calculate the A matrices of the remaining $m-1$ layers of the block, storing then temporarily in another file. We would then solve for the site potentials starting at the other end of the block and using either (3.4) (in that case we would have to find the B matrix at each layer, but that could be discarded when we moved to the next layer) or (3.5). The two files that must be used have sizes proportional to L_z/m and to m, and their combined total size is therefore minimized by choosing $m = \sqrt{L_z}$. We would then need to store only $2\sqrt{L_z}$ instead of L_z admittance matrices. The price paid is a doubling of the time spent in calculating the A matrices, since most of them would have to be calculated twice. The effect on the total amount of computer time would be less drastic, however, since most of the time is spent on the matrix inversion, i.e., on solution of (3.4) or (3.5).

The time spent on matrix inversion can in turn be reduced considerably by eliminating the dangling bonds from the percolating clusters. These are all the percolating cluster bonds that are not part of the backbone and therefore carry no current and have zero voltage across them. This can be done by the method of burning.[19] If this is not done, our

method requires inverting a large number of $L_x L_y \times L_x L_y$ matrices. This may be contrasted with the matrix inversion technique of ref. 14, where a single matrix of order $L_x L_y L_z \times L_x L_y L_z$ must be inverted. Clearly, since our method does not have to use numerical matrix inversion at its outer limits, far greater accuracy can be achieved in the solution for the site voltages.

We have used both (3.4) and (3.5) on different samples, and in a small number of cases we used both approaches on the same sample in order to check for consistency. In order to check the accuracy of each simulation we calculated the conductance G in three different ways, one of which does not depend upon the detailed voltage distribution: (i) From the admittance matrix of the entire strip, as described in the discussion following (3.2). (ii) From the total rate of production of Joule heat

$$G = \sum_a g_a V_a^2 \tag{3.6}$$

Here V_a is the calculated voltage across the bond a whose conductance is g_a. (iii) By using the fact that the total amount of current passing through each layer parallel to the external equipotential plates must equal the total external current. Thus

$$I_{\text{ext}} = \sum_a g_a V_a = G \tag{3.7}$$

Here the summation is over all the bonds whose direction is perpendicular to the plates, and the voltages can be either positive or negative. In all the cases, the agreement between the three calculated values of G was up to at least eight significant digits, indicating the accuracy of the method.

4. RESULTS OF THE SIMULATIONS

A number of different models were simulated: An ensemble of class 1 networks in the shape of a cube, i.e., $L_x = L_y = L_z \equiv L$ for $L \leqslant 15$, and an ensemble of class 2 networks, also in the shape of a cube, for $L \leqslant 25$. In order to avoid the errors which finite-size effects would introduce into any sequence of simulations with $p_1 \to p_c$, we performed all calculations at p_c. The results then depend on the linear size of the network L.

Originally we had also intended to simulate networks in the shape of a long strip, i.e., $L_x = L_y \ll L_z$. Such networks have the advantage that they are self-averaging, namely, for a sufficiently long strip a unique answer is obtained for given L_x, L_y. Thus, there would be no need to consider an ensemble of samples and choose between different ways of averaging the results. Unfortunately, the self-averaging is attained rather slowly with

increasing L_z, and we found that the memory requirements of the algorithm we had developed (see Section 3) prevent us from handling strips that are long enough.

For large enough L the asymptotic dependence of the Hall and Ohmic conductivities is a power law in L with exponents that are related to t, s, τ, and g by means of finite-size scaling. For an ensemble of samples of given linear size L and $\sigma_I/\sigma_M \ll L^{-(t+s)/\nu}$ (in this section we use σ_I, λ_I to denote the conductivities of the poor conductor, and σ_M, λ_M to denote those of the good conductor; ν is the correlation length exponent) the results for σ_e should cluster around two values, depending upon whether the sample does (regime I) or does not (regime II) percolate in the direction of the average electric field

$$\sigma_e \sim \begin{cases} \sigma_M & L^{-t/\nu} \quad \text{I} \\ \sigma_I & L^{s/\nu} \quad \text{II} \end{cases} \tag{4.1}$$

In the same ensemble, the results for λ_e are expected to cluster around three different values, depending upon whether the sample percolates in both directions perpendicular to H (I), in neither direction (II), or in just one of them (III). The expected behavior in each of these regimes can be deduced from the scaling form[6]

$$X \equiv \frac{\lambda_e - \lambda_I}{\lambda_M - \lambda_I} = \Delta p^{\tau} F\left(\frac{\sigma_I/\sigma_M}{\Delta p^{t+s}}\right) \tag{4.2}$$

by substituting $L^{-1/\nu}$ for Δp and noting that the fields $\mathbf{E}_0^{(e)}(\mathbf{r})$, $e = x, y$, $\mathbf{r} \in \sigma_M$, which appear in (2.8) scale with σ_I/σ_M as follows:

$$\mathbf{E}_0^{(e)}(\mathbf{r}) \sim \begin{cases} (\sigma_I/\sigma_M)^0 & \text{for} \quad \mathbf{r} \in \text{backbone} \\ (\sigma_I/\sigma_M)^1 & \text{for} \quad \mathbf{r} \notin \text{backbone} \end{cases} \tag{4.3}$$

From (4.3) we deduce the following asymptotic forms for the Hall conductivity scaling function $F(z)$:

$$F(z) \sim \begin{cases} \text{const} & \text{I} \\ z^2 & \text{II} \\ z & \text{III} \end{cases} \tag{4.4}$$

and consequently the following behavior for X as function of L for $p = p_c$:

$$X \sim \begin{cases} L^{-\tau/\nu} = L^{(g-2t)/\nu} & \text{I} \\ (\sigma_I/\sigma_M)^2 \, L^{(g+2s)/\nu} & \text{II} \\ (\sigma_I/\sigma_M) \, L^{(g+s-t)/\nu} & \text{III} \end{cases} \tag{4.5}$$

If we normalize X properly with the help of $\sigma_e^{(x)}$ and $\sigma_e^{(y)}$, the Ohmic conductivities in the two directions perpendicular to H (the averages of these conductivities should coincide, but for a specific disordered sample of finite size they will usually differ), we can make the expected critical exponents coincide in the three regimes

$$\frac{\sigma_M^2}{\sigma_e^{(x)}\sigma_e^{(y)}} X \sim L^{g/\nu} \qquad \text{I, II, III} \tag{4.6}$$

Finally, we note that if λ_I is small enough, namely if [see (2.14)]

$$\frac{\lambda_I}{\lambda_M} < \left(\frac{\sigma_I}{\sigma_M}\right)^2 L^{(2s+g)/\nu} \tag{4.7}$$

then

$$X \simeq \frac{\lambda_e}{\lambda_M}$$

$$\frac{\sigma_M^2}{\sigma_e^{(x)}\sigma_e^{(y)}} X \simeq \frac{R_e}{R_M} \tag{4.8}$$

In this section we will always implicitly assume that (4.7) holds. If it does not, then all the results we present are still valid if we replace λ_e/λ_M and R_e/R_M by the lhs of (4.8).

In the class 1, 3D models, each sample network in principle consists of a set of four simple cubic random bond networks that are electrically unconnected but strongly correlated. In using (B.16) to calculate λ_e it is easy to see that the sum separates into two parts—one involving two of these networks, the other involving the other two. Since the ensemble average or long strip average will be the same for all such pairs, it is enough to consider one pair, rather than all four networks, in each realization. In the class 2 models, every sample consists of just one, simple cubic (or simple square in 2D) independent random bond network.

In order to calculate the voltage distribution in a given sample, we imposed an appropriate fixed potential at sites on two opposite boundaries—say the x, z sides. At sites on the other sides, instead of imposing a linear potential variation as required by (B.5), we imposed the condition that no currents flow into the system. This may cause some concern, since the boundary condition (B.5), whereby the potential is prescribed at all boundary sites, was used in deriving (B.16), which we will ultimately use to evaluate λ_e. However, the altered boundary condition will affect the detailed votage distribution appreciably only near the boundaries. Thus, we may reasonably hope that we may still use (B.16) to get accurate results in the limit of large L.

For samples of finite L, one should nevertheless consider the effect of these incorrect boundary conditions, as well as of the fact that an individual sample at p_c often has very anisotropic electrical properties, thus casting some doubt upon the use of expressions like (2.7), (2.8) [or their discrete analogues (B.15), (B.16)], (2.12), and (4.8). In the general case of an anisotropic sample, it follows from our boundary conditions that the Ohmic quantities which we compute $\sigma_e^{(x)}$, $\sigma_e^{(y)}$ are really $1/\rho_{exx}$, $1/\rho_{eyy}$, i.e., the reciprocals of two diagonal elements of the Ohmic resistivity tensor $\ddot{\boldsymbol{\rho}}_e \equiv (\ddot{\boldsymbol{\sigma}}_e)^{-1}$. Similarly, the Hall quantity λ_e that we compute for a single sample using (2.8) or (B.16) is really just the z component of the full vector $\boldsymbol{\lambda}_e$, which usually does not lie along $\mathbf{H} \| z$. If we had wanted to calculate the z component of the Hall resistivity vector $\mathbf{R}_e$ from a knowledge of $\ddot{\boldsymbol{\rho}}_e$ and $\boldsymbol{\lambda}_e$, we would have found (here we omit the subscript e for the purpose of clarity)

$$R_z = \lambda_z(\rho_{xx}\rho_{yy} - \rho_{xy}^2) + \lambda_x(\rho_{xy}\rho_{yz} - \rho_{yy}\rho_{xz}) + \lambda_y(\rho_{xy}\rho_{xz} - \rho_{xx}\rho_{yz}) \quad (4.9)$$

for small H, instead of the result of (4.8), which we can now rewrite as

$$R_e = \lambda_{ez}\rho_{exx}\rho_{eyy} \quad (4.10)$$

As far as the quantity λ_{ez} is concerned, arithmetical averaging over the ensemble (which is what we used) should make things right because the other components λ_{ex}, λ_{ey} will average to zero if the ensemble is isotropic or cubic. This remains true even if we average only over the partial ensemble corresponding to one of the groups of samples 1–4 of Fig. 5.[6] In this averaging process R_{ex}, R_{ey}, ρ_{eij}, $i \neq j$, will also average to zero. The only remaining question is whether the average of the calculated R_e of (4.10)

[6] To see this, consider what happens when a sample network is reflected through an x, z plane, i.e., along the y axis. Denoting the voltages of the original and the reflected network on corresponding bonds by $V_a^{(e)}$, $\tilde{V}_a^{(e)}$, respectively, it is easy to see that

$$\tilde{V}_a^{(y)} = V_a^{(y)}, \quad \tilde{V}_a^{(x)} = -V_a^{(x)}, \quad \tilde{V}_a^{(z)} = -V_a^{(z)} \quad \text{for} \quad a \| y$$

$$\tilde{V}_a^{(y)} = -V_a^{(y)}, \quad \tilde{V}_a^{(x)} = V_a^{(x)}, \quad \tilde{V}_a^{(z)} = -V_a^{(z)} \quad \text{for} \quad a \perp y$$

From this and from (B.14) it follows that λ_{ey} and σ_{exy} both change sign for the reflected network. Since the original and the reflected network belong to the same ensemble, the arithmetic averages of λ_{ey} and σ_{exy} must vanish, even when the average is restricted to one of the groups 1–4 of Fig. 5. Similar considerations can be applied to show that the last two terms of (4.9) also vanish. For example, in the product $\lambda_{ey}\rho_{exy}\rho_{exz}$, all three factors change sign under reflection along y, while in the product $\lambda_{ey}\rho_{exx}\rho_{eyz}$ only the last factor changes sign under reflection along z.

matches with the average of the true z component R_{ez} of (4.9). It can be shown that the last two terms of (4.9) average to zero separately in each of the groups 1–4 of Fig. 5 (see footnote 6). The average of (4.9) thus becomes

$$\langle R_e \rangle = \langle \lambda_{ez}(\rho_{exx}\rho_{eyy} - \rho_{exy}^2) \rangle \tag{4.11}$$

and this differs from the average of (4.10) due to the appearance of $\lambda_{ez}\rho_{exy}^2$, which does not average to zero. Since we did not calculate the off-diagonal element of the resistivity tensor ρ_{exy}, we could not calculate (4.11), but we expect that $\lambda_{ez}\rho_{exy}^2$ will scale with L in the same way as $\lambda_{ez}\rho_{exx}\rho_{eyy}$, and therefore that (4.11) will have the same critical behavior as (4.10).

In order to verify this expectation, we also calculated R_e in a different way: We first averaged the results for $1/\rho_{exx}$, $1/\rho_{eyy}$, λ_{ez} over all samples with a given L (in the case of the class 2 model this was done separately for each group 1–4 of Fig. 5), and then used (4.10) to calculate R_e for that L. Since, in this averaging procedure, λ_{ex}, λ_{ey}, ρ_{eij}, $i \neq j$, should all average to zero, (4.10) then yields the correct (average) value of R_e. We shall see below that as far as the scaling behavior is concerned, the results of this procedure are in full agreement with those obtained by using (4.10) for each sample individually.

4.1. Class 1 Cubic-Shaped Networks

A single layer, perpendicular to z, of such a network with $L = 3$ is shown in Fig. 4. The network consists of two unconnected simple networks P and D (standing for primal and dual), one of which (D) is connected to the external world in the x direction, while the other (P) is similarly connected in the y direction. The x and y bonds in one layer of either P or D form a 2D independent random bond network, but there are strong correlations between P and D: The two simple square networks that appear in every x, y planar cross section are mutually dual.

Applying an external potential difference in the y direction, we determine the Ohmic conductivity σ_e of the network P, as well as the detailed voltage distribution on all its conductors. Similarly, by applying a potential difference in the x direction we determine the conductivity σ_{eD} of the network D as well as its detailed voltage distribution. The two voltage distributions are then used in (B.16) to calculate the Hall conductivity λ_e. When this is done for samples in which each conductor is either $g_M = 1$ or $g_I = 0$, and the fraction of g_M's is equal to the percolation threshold, most of the samples (about 3/4) will have a zero value for λ_e and for at least one of the two Ohmic conductances. However, if we assign a small but nonzero

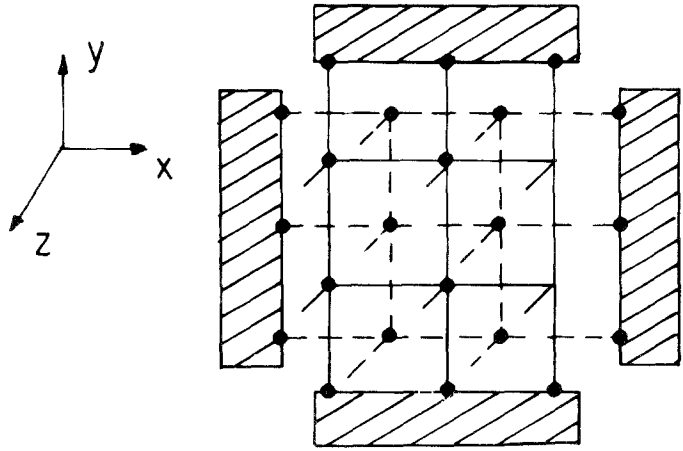

Fig. 4. One x, y layer of a class 1 model showing the two electrically unconnected networks (solid lines and dashed lines). An x bond from one network is equal to the y bond from the other network that intersects it. Thus, the x and y bonds of both networks form a self-dual array. The z bonds from the two networks are uncorrelated. Clearly, the solid-line network determines $\sigma_e^{(y)}$ while the dashed-line network determines $\sigma_e^{(x)}$. Both networks determine λ_e.

value to g_1, say $g_1 = 10^{-8}$, all three conductances will have nonzero values, and we can always calculate the Hall coefficent R_e from [see (4.8)]

$$HR_e = \frac{\lambda_e}{\sigma_e \sigma_{eD}} \tag{4.12}$$

The price paid for taking $g_1 \neq 0$ is that the transfer matrix calculations are slower: When $g_1 = 0$, the calculation is speeded up considerably because in many cases most of the elements of the admittance matrix do not have to be updated even though a new bond is being added to the network. This occurs whenever the new bond is being attached to a site that is unconnected to any other site (see ref. 11).

The results of such a set of calculations for an ensemble of cubic samples of size $L_x \times L_y \times L_z = 8^3$ are shown in Figs. 5a and 5b, where we exhibit plots of $\ln \sigma_e$ vs. $\ln \sigma_{eD}$ and $\ln |\lambda_e|$ vs. HR_e, respectively. In Fig. 5a, where both axes are logarithmic, the points are bunched into four very separate groups. Group 1 corresponds to samples where both P and D percolate, group 2 to samples where neither percolates, and group 3 (4) to samples where only P (D) percolates. Within groups 1, 3 and 4 there appears to be no correlation between the deviations of σ_e and σ_{eD} from their average values, and the average value for a particular subnetwork (P or D) depends only on whether it percolates. In group 2 there appears

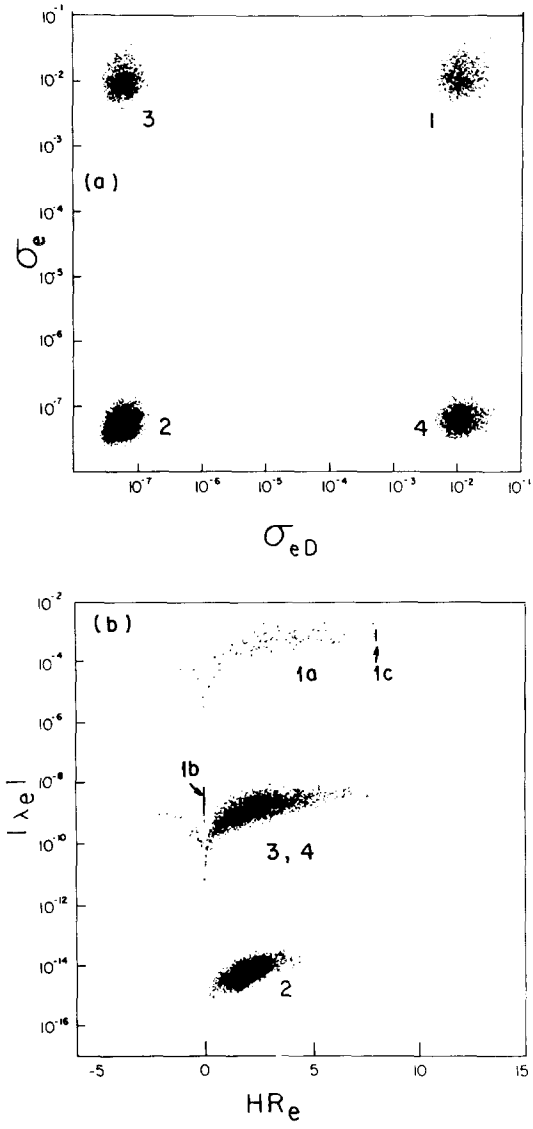

Fig. 5. (a) Plot of $\ln \sigma_e$ vs. $\ln \sigma_{eD}$ for an ensemble of class 1 $8 \times 8 \times 8$ samples: The four clusters of points 1–4 correspond, respectively, to samples where both subnetworks P and D percolate, where neither percolates, where only P percolates, and where only D percolates. Within groups 1, 3, and 4 there appears to be no correlation between the fluctuations of σ_e and σ_{eD} about their average values, while within group 2 there is some positive correlation. (b) Plot of $\ln |\lambda_e|$ vs. HR_e for the same ensemble. Note that λ_e and R_e are negative for some samples, even though $\langle \lambda_e \rangle$ and $\langle R_e \rangle$ are always positive. The bottom cluster corresponds to group 2 of (a). The top cluster contains samples coming only from group 1 of (a). The middle cluster contains all the samples from groups 3 and 4 of (a), as well as those samples from group 1 (denoted as 1b) that either have no binodes or have mutually canceling pairs of binodes. In the top cluster we have denoted by 1a the generic samples, and by 1c those that result in $R_e = L = 8$.

to be some correlation between those deviations. This is apparent from the skewed shape of the distribution of points. This correlation is probably due to the great sensitivity of a nearly percolating network to close encounters between different clusters, and hence to local enhancements of the fraction p_M of the good conductors.

In Fig. 5b, where only the $|\lambda_e|$ axis is logarithmic, the points separate vertically into three main groups. While those groups differ greatly in their values of λ_e, they all span similar ranges in R_e. The samples that contribute to the lower group are those that formed group 2 in Fig. 5a—the doubly nonpercolating samples. The samples contributing to the upper group are those from group 1 (the doubly percolating samples) that have binodes, i.e., points of intersection between the backbone of P and that of D. This group is denoted by 1a. The contributors to the middle group are all the samples from groups 3 and 4 (the singly percolating samples) plus those samples from group 1, called 1b, that either lack binodes or have binodes whose contributions cancel each other (see the discussion below).

In the upper group there is a concentration of points, called 1c, at $HR_e = L = 8$. This comes mainly from samples where the percolating backbone in both P and D is composed of one singly connected chain, and these intersect at a site where both currents are in the x–y plane. Such an intersection is called positive if the currents are either both in the positive direction or both in the negative direction, thus making a positive contribution to λ_e. Otherwise, the intersection is called negative. (Note that even though the ensemble average of λ_e or R_e is positive, an individual sample can lead to negative values.) Denoting the lengths of the two chains by $\mathscr{L}_P$ and $\mathscr{L}_D$, the Ohmic conductivities are

$$\sigma_e = \frac{1}{L\mathscr{L}_P}, \qquad \sigma_{eD} = \frac{1}{L\mathscr{L}_D} \tag{4.13}$$

while the Hall conductivity and Hall coefficient are easily seen to be

$$\lambda_e = \pm \frac{1}{L\mathscr{L}_P\mathscr{L}_D}, \qquad RH_e = \pm L \tag{4.14}$$

The same result is obtained even if the backbone of the second subnetwork is made of more than one singly connected chain, but each of these has one intersection with the single chain in the first subnetwork and the intersections are all either positive or negative. If there are equal numbers of positive and negative binodes, a cancellation occurs and such samples also contribute to the subgroup 1b of Fig. 5b. In practice, this concentration of results at $HR_e = L$ was not observed for $L > 10$.

In order to analyze these results using finite-size scaling, we note that even though the λ_e values separate into three groups that differ by many orders of magnitude and should also scale differently with L, the values of R_e are all concentrated in one group and should scale in the same way [see Fig. 5b and (4.5), (4.6), (4.8)]

$$\frac{R_e}{R_M} \simeq \frac{\sigma_M^2}{\sigma_e \sigma_{eD}} \frac{\lambda_e}{\lambda_M} \sim L^{g/\nu} \tag{4.15}$$

when

$$\frac{\sigma_I}{\sigma_M} \ll L^{-(t+s)/\nu} \qquad \text{and} \qquad \frac{\lambda_I}{\lambda_M} \ll \left(\frac{\sigma_I}{\sigma_M}\right)^2 L^{(2s+g)/\nu}$$

However, since the coefficient of proportionality that is implied in (4.15) need not be the same above and below p_c, we analyzed the results for λ_e/λ_M and R_e/R_M separately for the groups 1, 2, and 3 + 4, as well as for all the groups together. When treated separately, those three groups yielded the values (see Fig. 6a)

$$g/\nu = \begin{cases} 0.41 \pm 0.05 & \text{group 1} \\ 0.26 \pm 0.03 & \text{group 2} \\ 0.28 \pm 0.05 & \text{group 3} + 4 \end{cases} \tag{4.16}$$

and the coefficient of proportionality was different in each case. We then introduced a multiplicative factor for the group 2 results and another one for the group 3 + 4 results, which were adjusted to bring them as much as possible in line with the group 1 results. In this way we found (see Fig. 6b)

$$g/\nu = 0.31 \pm 0.04 \qquad \text{all groups} \tag{4.17}$$

These results were obtained by first calculating R_e for each sample using (4.8) or (4.10) and then averaging over the ensemble. We also calculated $\langle R_e \rangle$ by first averaging $1/\rho_{exx}$, $1/\rho_{eyy}$, λ_{ez} over the samples in each group 1–4 of Fig. 5 and then using (4.10). The results for g/ν were the same.

In Fig. 7, we also plot the values of $\ln\langle \lambda_e \rangle$ vs. $\ln L$, from which we obtained a direct calculation of the critical exponent $\tau = 2t - g$,

$$\tau/\nu = 4.3 \pm 0.2 \tag{4.18}$$

Obviously, in this calculation only the samples of groups 1a and 1c make a contribution. Finally, in Fig. 8, we plot the Ohmic conductivities $\ln\langle \sigma_e \rangle$ and $\ln\langle \sigma_{eD} \rangle$ vs. $\ln L$, and obtain for the critical exponent t

$$t/\nu = 2.29 \pm 0.04 \tag{4.19}$$

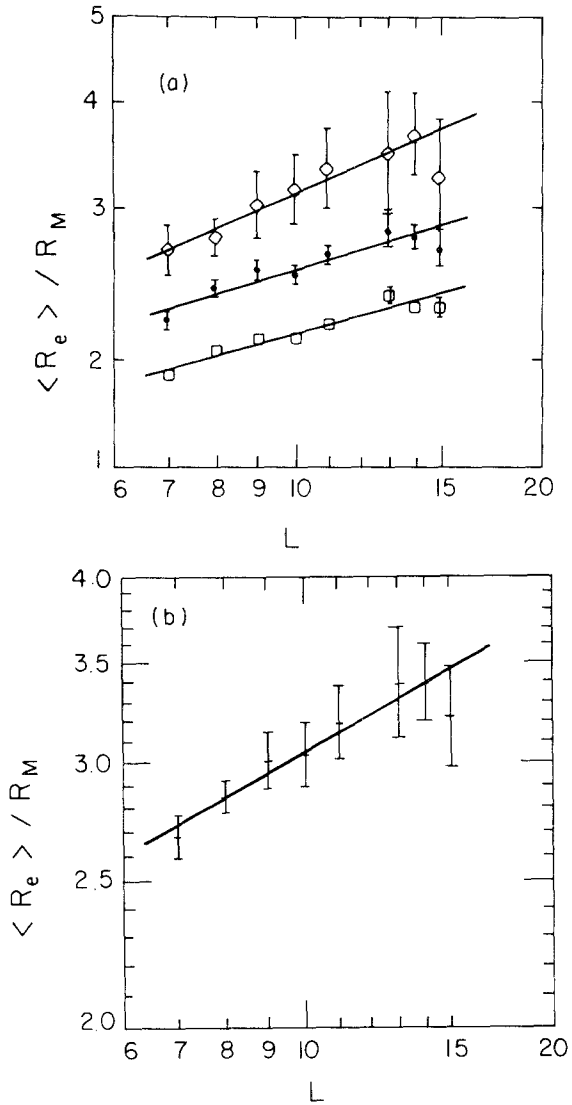

Fig. 6. (a) Plots of $\ln(\langle R_e \rangle / R_M)$ vs. $\ln L$ separated according to the degree of percolation: The top points come from averages of R_e over doubly percolating samples (group 1 of Fig. 5a), the middle points come from singly percolating samples (groups 3 + 4), the bottom points come from nonpercolating samples (group 2). The straight lines are weighted least-squares fits to the respective data, where the weight of each point is the reciprocal of the estimated error. The error bars in this and in all subsequent figures are obtained by dividing the rms or standard deviation of each point by $\sqrt{n}$, where n is the number of samples used to calculate that point. (b) Same as (a), but now all samples are considered together after renormalizing the two lower sets of points from (a) by appropriate multiplicative constants. The straight line is a weighted least-squares fit.

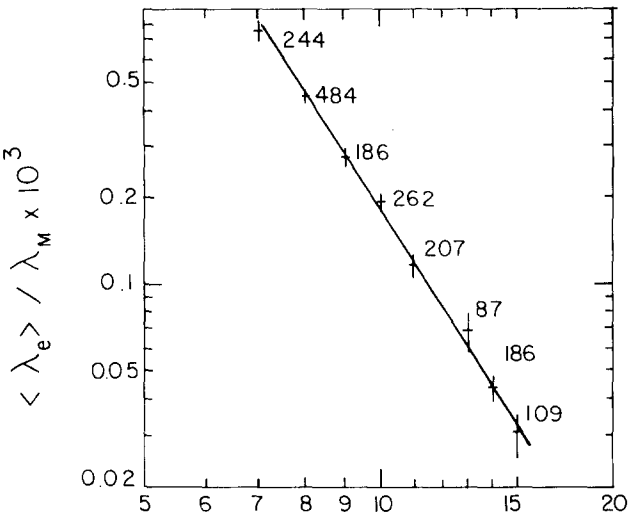

Fig. 7. Plot of $\ln(\langle \lambda_e \rangle / \lambda_M)$ vs. $\ln L$ for class 1 cubic-shaped samples. The straight line is a weighted least-squares fit. The number appearing next to each point is the number of doubly percolating samples n used to calculate that point and its error bar. The same samples were also used to calculate the upper points in Fig. 6a and all the points of Fig. 9.

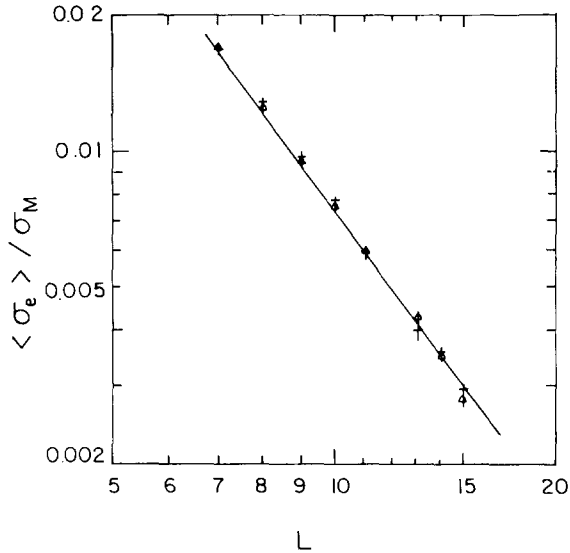

Fig. 8. Plot of (+) $\ln(\langle \sigma_e \rangle / \sigma_M)$ and (Δ) $\ln(\langle \sigma_{eD} \rangle / \sigma_M)$ vs. $\ln L$ for class 1 cubic-shaped samples. The straight line is a weighted least-squares fit. In this case, both singly and doubly percolating samples were used to calculate each point.

The good agreement of this result with previously published values[17] of t/ν gives us confidence in the accuracy of the simulations and their analysis.

The fact that the values of g/ν obtained from the different groups of samples seem to be somewhat different, even though the scaling theory predicts that they should agree, may arise from the following causes: (a) These simulations were all done at $p_c = 0.2492$, which is correct for an infinite network. For finite networks, if p_c is defined as the value of p where half of the samples percolate, then p_c depends on L and only approaches the above value asymptotically.[20] (b) In those samples in which λ_e and either σ_e or σ_{eD} (or both) are small, the precise values depend on the voltages across conducting (σ_M) bonds that form finite clusters. Those voltages are very small [i.e., of order σ_I/σ_M—see (4.3)] and are obtained as differences between the large but nearly equal potentials at their ends. Thus, their accuracy is considerably lower than that of the voltages on bonds of the percolating backbones which determine the conductivities in samples where λ_e, σ_e, σ_{eD} are all large.

As a byproduct of these simulations, we also obtained the density of binodes $\rho_{BN} \equiv N_{BN}/N$ in our samples; this is plotted in Fig. 9 vs. L on a log–log plot, and leads to the conclusion that

$$\rho_{BN} \sim L^{-b}, \qquad b = 2.2 \pm 0.1 \tag{4.20}$$

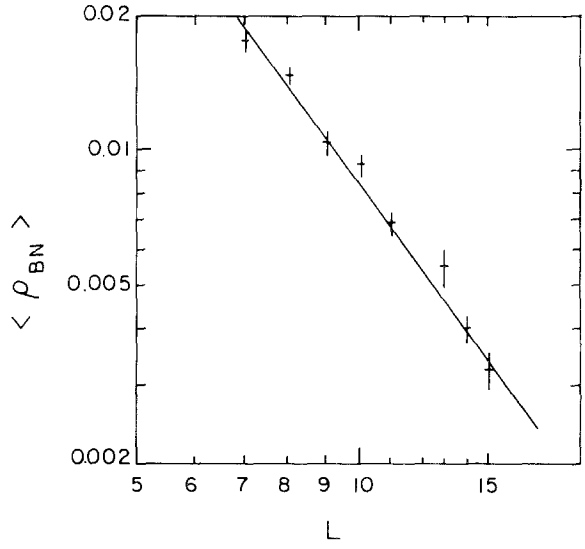

Fig. 9. Plot of $\ln\langle\rho_{BN}\rangle$, the density of binodes in cubic-shaped class 1 samples, vs. $\ln L$. The straight line is a weighted least-squares fit.

On each of the networks P and D the density of backbone bonds at p_c should behave as $L^{D_B - d}$, where $d=3$ is the dimensionality of our samples and $D_B = 1.77 \pm 0.07$ is the fractal dimensionality of the backbone.[19] If the two networks were uncorrelated, we would expect ρ_{BN} to be the square of the backbone density, i.e.,

$$\begin{aligned} \rho_{BN} &\sim L^{-2(d-D_B)} \\ 2(d-D_B) &= 2.46 \pm 0.14 \end{aligned} \tag{4.21}$$

The fact that b is somewhat smaller than that should therefore be ascribed to the positive correlation between the backbones of P and D. That is, when a bond a belongs to the backbone of P, then not only is its intersecting bond $\tilde{a}$ a conducting bond of D, but in its neighborhood there are more conducting bonds of D than would be present near a conducting bond chosen at random. From (4.20) we conclude that the fractal dimension of the set of binodes is

$$D_{BN} = d - b = 0.8 \pm 0.1 \tag{4.22}$$

4.2. Class 2 Cubic-Shaped Networks

An ensemble of samples was simulated for each value of $L \leqslant 25$ in order to calculate $\langle \lambda_e \rangle$, $\langle \sigma_e \rangle$, and $\langle R_e \rangle$. Each sample was an independent, random bond, simple cubic network. An x, y layer in such a sample is shown for $L=4$ in Fig. 10. A total of L such planes are stacked per-

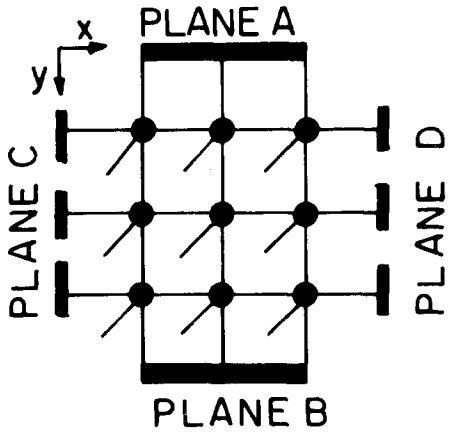

Fig. 10. One x–y layer of a class 2 sample of linear size $L=4$. The total number of layers stacked together to form the entire network is also L.

pendicular to the z axis, so that the linear size in that direction is also L. In order to calculate the voltage distribution when the average electric field is the unit vector $\mathbf{e}_y$, we thus apply a potential difference equal to L between the x, z sides of the network.

Another point to consider is what value we should use in (B.16) for N, the total 3D size of the system. We used the value that gives the correct answer [namely, $(\lambda_e - \lambda_I)/(\lambda_M - \lambda_I) = 1$] for the uniform network, namely

$$N_\lambda = L(L-1)^2 \tag{4.23}$$

We also calculated the conductivity σ_e in such a way that the correct answer was regained for the uniform network, for example

$$\sigma_e = \frac{L}{L(L-1)} G_e = \frac{G_e}{L-1} \tag{4.24}$$

where G_e is the total conductance. Note that if we use (B.15) to calculate this conductivity, we must use a different value of N, namely

$$N_\sigma = L^2(L-1) \tag{4.25}$$

in order to get the right answer for a uniform network.

In order to determine asymptotic critical behaviors, all the samples of size L were produced with the help of a quasirandom-number generator using an occupation probability for individual bonds equal to[20]

$$p_c(L) = 0.2492 + 0.071L^{-1/\nu} + 1.25L^{-2/\nu}, \qquad \nu = 0.88 \tag{4.26}$$

This is the percolation threshold adjusted for the particular value of L, i.e., at $p = p_c(L)$ one-half of the samples produced in a large ensemble percolate in a given direction.

Finally, in order to look for power law behavior in $\langle \sigma_e \rangle$, $\langle \lambda_e \rangle$, $\langle R_e \rangle$ as functions of linear size, we had to choose an appropriate linear size: Because of the nature of our samples, there is some ambiguity in this choice and one may use either L or $L-1$, or some other intermediate value such as $N_\sigma^{1/3}$ or $N_\lambda^{1/3}$. We have chosen to use L. While this will not make any difference for large L, it may affect the calculation of power law exponents at finite L.

The results for $\langle \sigma_e \rangle$, $\langle \lambda_e \rangle$, $\langle R_e \rangle$ vs. L are plotted in Figs. 11–13 on a log–log scale. In plotting $\langle R_e \rangle$, we only used doubly percolating samples, since in these calculations we put $g_I = 0$ [compare with the discussion preceding (4.12)]. In Fig. 14 we also plot the total number of backbone bonds N_B (i.e., the total number of current-carrying bonds) vs. L. The expected dependence of N_B on L is $N_B \sim L^{D_B}$, where $D_B = 1.77 \pm 0.07$ is the

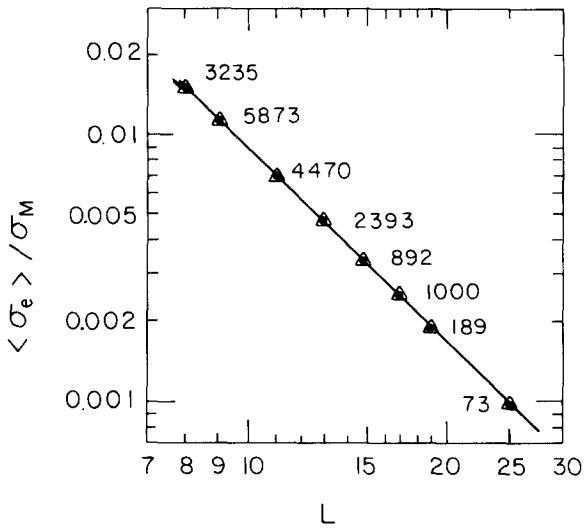

Fig. 11. Plot of (●) $\ln(\langle\sigma_e^{(x)}\rangle/\sigma_M)$ and (△) $\ln(\langle\sigma_e^{(y)}\rangle/\sigma_M)$ for class 2 cubic-shaped samples vs. ln L. The straight line is a weighted least-squares fit. The number appearing next to each pair of points is the total number of doubly percolating samples used to calculate that pair. The same samples were also used to calculate the points in Figs. 12–14.

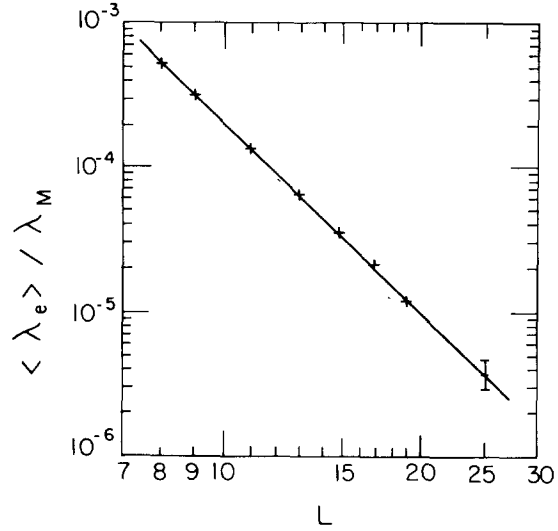

Fig. 12. Plot of $\ln(\langle\lambda_e\rangle/\lambda_M)$ vs. ln L for class 2 cubic-shaped samples. The straight line is a weighted least-squares fir.

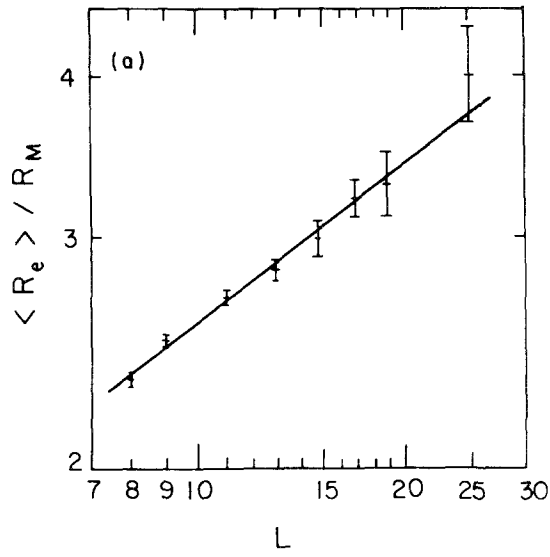

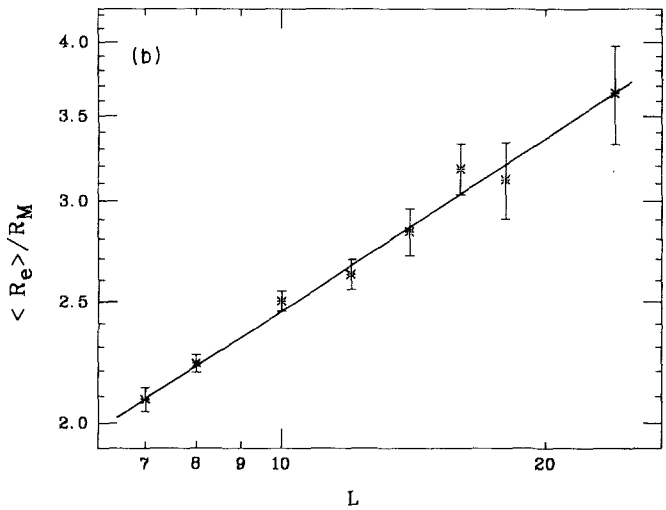

Fig. 13. Log–log plots of $\langle R_e \rangle / R_M$ vs. L for class 2 cubic-shaped samples. The straight lines are weighted least-squares fits. (a) R_e was calculated for each individual sample using (4.8) or (4.10), then averaged over all samples with the same L. (b) R_e was calculated for each value of L from the averaged values of $1/\rho_{exx}$, $1/\rho_{eyy}$, λ_{ez} using (4.10).

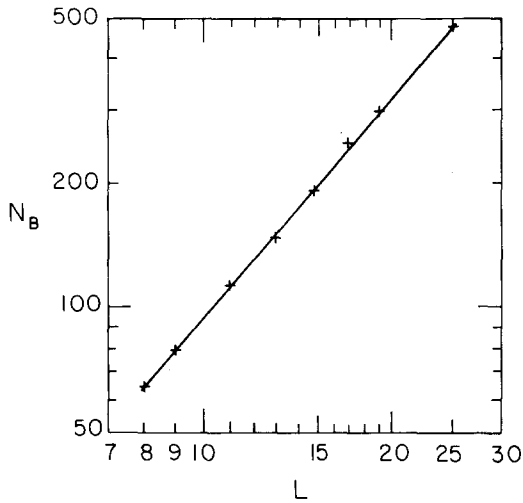

Fig. 14. Plot of ln N_B, the size of the backbone, vs. ln L for class 2 cubic-shaped samples. The straight line is a weighted least-squares fit.

fractal dimension of the percolating backbone.[19] From these results we determined the following values for the critical exponents

$$\begin{aligned} D_B &= 1.72 \pm 0.02 \\ t/\nu &= 2.37 \pm 0.02 \\ \tau/\nu &= 4.35 \pm 0.04 \\ (g/\nu)_1 &= 0.42 \pm 0.03 \\ (g/\nu)_2 &= 0.40 \pm 0.05 \end{aligned} \tag{4.27}$$

where the two values for g/ν were obtained by using different procedures for the calculation of $\langle R_e \rangle$: $(g/\nu)_1$ was obtained by using (4.8) or (4.10) to calculate R_e for each sample, then R_e was averaged arithmetically over all samples for given L. The value of $(g/\nu)_2$ was obtained by using (4.10) with the (arithmetic) average values of $1/\rho_{exx}$, $1/\rho_{eyy}$, λ_{ez}, as explained earlier in this section. These values and errors were obtained by a weighted least squares fit. The fact that our value for D_B is in good agreement with the above quoted result can serve as some indication of the accuracy of our results. The fact that our value for t/ν is a little higher than the result $t/\nu = 2.2 \pm 0.1$ of Ref. 17 may be due to the fact that we included only the doubly percolating samples in our calculation.

5. SUMMARY AND DISCUSSION

We have described extensive simulations made for the purpose of studying the critical properties of the weak-field Hall effect near a percolation threshold. Two different network models were used that lead to the correct behavior of the bulk effective Hall coefficient R_e in 2D systems, as known from an exact theorem. In 3D systems these models yielded the following results regarding the critical behavior of R_e:

$$\begin{aligned} &R_e \sim L^{g/\nu} \\ &g/\nu = 0.41 \pm 0.05 \qquad \text{for class 1 model} \\ &g/\nu = 0.42 \pm 0.03 \qquad \text{for class 2 model} \end{aligned} \tag{5.1}$$

Here we have quoted the result from the class 1 model only for doubly percolating samples, which are also the only kinds of samples that were considered for the class 2 model. In order to obtain reliable results from the other types of samples, we would need to analyze carefully the errors incurred in calculating the very small voltages on conducting bonds that do not belong to the backbone. It is actually possible to do this with the help of the algorithm described in Section 3, which enables us to find all the bond voltages with unprecedented accuracy. This is currently being studied in connection with the detailed voltage distribution on bonds of these networks and will be discussed elsewhere.[12] A certain discrepancy appears if we compare the above results to those of ref. 8, where it was found that $g = 0.29 \pm 0.05$, which translates to ($\nu = 0.89 \pm 0.01$; see ref. 21)

$$g/\nu = 0.33 \pm 0.05$$

Other recent calculations also lead to a value for g/ν that is not in very good agreement with our results.[22]

Some of these discrepancies can probably be ascribed to systematic errors that are not included in the quoted errors—those include statistical errors only. Systematic errors may arise from the use of incorrect boundary conditions, from using an incorrect linear size L to characterize the finite samples, or simply from using values of L that are not large enough to ensure correct asymptotic behavior. Some of these problems can perhaps be alleviated by performing the simulations at $p = p_c(L)$ [see (4.26)] instead of at $p = p_c(\infty)$. This was recognized too late to be used in the class 1 model, but was implemented in the class 2 model. The results from ref. 8 probably suffer from systematic errors due to finite-size effects, since those calculations were done on networks at $p \neq p_c$.

Another annoying feature is the apparent discrepancy between values of g/ν obtained from class 1 samples with different percolation charac-

teristics. If true, this would violate the scaling theory predictions. We believe that these discrepancies are again due to the use of a fixed value for p_c rather than $p_c(L)$, as well as to the errors associated with calculating the very small bond voltages which we alluded to before.

It would be highly desirable to develop a network model for the Hall effect that is not restricted to weak magnetic fields and that does not suffer from the appearance of unphysical binodes. Such a model might serve not only to get better results for the weak-field exponent g, but also to perform simulations of the Hall effect and magnetoresistance in strong magnetic fields. Such a model has recently been suggested,[23] and will be used to perform further studies.

APPENDIX A. THEORY OF THE LOW-FIELD HALL EFFECT IN A CONTINUUM COMPOSITE MEDIUM

In order to calculate the local electric field $\mathbf{E}(\mathbf{r}) = -\nabla\phi(\mathbf{r})$ in a continuum composite medium in the presence of a constant magnetic field $\mathbf{H}$, we must solve a boundary value problem with a linear partial differential equation

$$\begin{aligned} 0 = \nabla \cdot \mathbf{J}(\mathbf{r}) = & -\nabla \cdot \sigma_0[1 - u_\theta(\mathbf{r})]\,\nabla\phi(\mathbf{r}) + \nabla \cdot [\boldsymbol{\lambda}(\mathbf{r}) \times \nabla\phi(\mathbf{r})] \\ & \phi(\mathbf{r}) = \phi_{00}(\mathbf{r}) \text{ on the surface of the sample} \end{aligned} \tag{A.1}$$

We should think of the composite as comprised of $n+1$ isotropic components, each with its own Ohmic and Hall conductivities σ_i, $\boldsymbol{\lambda}_i \| \mathbf{H}$, $i = 0, 1, 2, \ldots, n$. In (A.1) we have artificially separated out the σ_0 component and are treating it as the host. With the help of the characteristic step functions

$$\theta_i(\mathbf{r}) = \begin{cases} 1 & \text{if } \mathbf{r} \text{ is inside the } \sigma_i \text{ component} \\ 0 & \text{otherwise} \end{cases} \tag{A.2}$$

we can write

$$\begin{aligned} \sigma(\mathbf{r}) = \sum_{i=0}^{n} \sigma_i \theta_i &= \sigma_0 \left[1 - \sum_{i=1}^{n} (1 - \sigma_i/\sigma_0)\,\theta_i \right] \\ &\equiv \sigma_0[1 - u_\theta(\mathbf{r})] \end{aligned} \tag{A.3}$$

which serves to define the function $u_\theta(\mathbf{r})$ that appears in (A.1). The function $\phi_{00}(\mathbf{r})$, which provides the boundary values of $\phi(\mathbf{r})$, will always be taken to be a solution of Laplace's equation that leads to a uniform electric field of unit amplitude, e.g.,

$$\begin{aligned} \phi_{00}^{(e)}(\mathbf{r}) &= -\mathbf{e} \cdot \mathbf{r} \\ \mathbf{E}_{00}^{(e)} &\equiv -\nabla\phi_{00} = \mathbf{e} \end{aligned} \tag{A.4}$$

When this boundary condition is chosen, the solution of (A.1) is denoted by $\phi^{(e)}(\mathbf{r})$. The resulting current density [see (2.1)] is then denoted by $\mathbf{J}^{(e)}(\mathbf{r})$, while the solution of (A.1) in zero magnetic field, i.e., when $\lambda(\mathbf{r}) \equiv 0$, is denoted by $\phi_0^{(e)}(\mathbf{r})$.

With the help of the Green's function $G(\mathbf{r}, \mathbf{r}' \mid u_\theta)$, defined by

$$\begin{gathered} \nabla \cdot [1 - u_\theta(\mathbf{r})] \nabla G(\mathbf{r}, \mathbf{r}') = -\delta^d(\mathbf{r} - \mathbf{r}') \\ G = 0 \text{ on the surface of the sample} \end{gathered} \tag{A.5}$$

(d is the dimensionality, in practice either $d=2$ or $d=3$), we can transform (A.1) in the usual way to a linear integral equation for ϕ,

$$\begin{aligned} \phi(\mathbf{r}) &= \phi_0(\mathbf{r}) - \frac{1}{\sigma_0} \int dV'\, G(\mathbf{r}, \mathbf{r}') \nabla' \cdot [\lambda(\mathbf{r}') \times \nabla' \phi(\mathbf{r}')] \\ &= \phi_0(\mathbf{r}) - \frac{1}{\sigma_0} \int dV'\, \lambda(\mathbf{r}') \cdot [\nabla' G(\mathbf{r}, \mathbf{r}') \times \nabla' \phi(\mathbf{r}')] \end{aligned} \tag{A.6}$$

where $\phi_0(\mathbf{r})$ is the solution of (A.1) for $\lambda(\mathbf{r}) \equiv 0$. The last line of (A.6) was obtained by integrating by parts and using the boundary condition $G = 0$.

Before continuing, we note that G_0, which is simply G for the case when $\sigma(\mathbf{r}) \equiv \sigma_0$, i.e., $u_\theta(\mathbf{r}) \equiv 0$,

$$G_0(\mathbf{r}, \mathbf{r}') \equiv G(\mathbf{r}, \mathbf{r}' \mid u_\theta \equiv 0) \tag{A.7}$$

can be used to write integral equations for $\phi_0(\mathbf{r})$ and for G itself: Starting with the boundary value problem (A.1) with $\lambda(\mathbf{r}) \equiv 0$, we can transform it in the usual way to

$$\begin{aligned} \phi_0(\mathbf{r}) &= \phi_{00}(\mathbf{r}) - \frac{1}{\sigma_0} \int dV'\, G_0(\mathbf{r}, \mathbf{r}') \nabla' \cdot [\sigma_0 u_\theta(\mathbf{r}') \nabla' \phi_0(\mathbf{r}')] \\ &= \phi_{00}(\mathbf{r}) + \int dV'\, u_\theta(\mathbf{r}') \nabla' G_0(\mathbf{r}, \mathbf{r}') \cdot \nabla' \phi_0(\mathbf{r}') \end{aligned} \tag{A.8}$$

In the same way, the problem (A.5) can be transformed into

$$G(\mathbf{r}, \mathbf{r}' \mid u_\theta) = G_0(\mathbf{r}, \mathbf{r}') + \int dV''\, u_\theta(\mathbf{r}'') \nabla'' G_0(\mathbf{r}, \mathbf{r}'') \cdot \nabla'' G(\mathbf{r}'', \mathbf{r}' \mid u_\theta) \tag{A.9}$$

Defining the linear operators Γ, Γ_0 by

$$\begin{aligned} \Gamma f &\equiv \int dV'\, u_\theta(\mathbf{r}') \nabla' G(\mathbf{r}, \mathbf{r}' \mid u_\theta) \cdot \nabla' f(\mathbf{r}') \\ \Gamma_0 f &\equiv \int dV'\, u_\theta(\mathbf{r}') \nabla' G_0(\mathbf{r}, \mathbf{r}') \cdot \nabla' f(\mathbf{r}') \end{aligned} \tag{A.10}$$

for an arbitrary function $f(\mathbf{r})$, we can rewrite (A.8) and (A.9) symbolically as

$$\begin{aligned} \phi_0 &= \phi_{00} + \Gamma_0 \phi_0 \\ G &= G_0 + \Gamma_0 G \end{aligned} \tag{A.11}$$

and consequently also

$$\Gamma = \Gamma_0 + \Gamma_0 \Gamma \tag{A.12}$$

These equations may be solved symbolically to yield

$$\begin{aligned} \phi_0 &= \frac{1}{1-\Gamma_0} \phi_{00} \\ \Gamma &= \frac{1}{1-\Gamma_0} \Gamma_0 \end{aligned} \tag{A.13}$$

and hence

$$\phi_0 = (1+\Gamma)\,\phi_{00} \tag{A.14}$$

Since both and G and G_0 are symmetric in their arguments, both Γ and Γ_0 are self-adjoint when u_θ is real.

Equation (A.6) can be solved to first order in H by replacing $\phi(\mathbf{r})$ on the rhs by $\phi_0^{(e)}(\mathbf{r})$. When this is substituted in (2.1), the volume average of the component of $\mathbf{J}^{(e)}(\mathbf{r})$ along the unit vector $\mathbf{f}$ can be written, up to order H^1, as

$$\begin{aligned} \langle \mathbf{J}^{(e)} \cdot \mathbf{f} \rangle = \langle & -\sigma(\nabla \phi_0^{(e)} \cdot \mathbf{f}) \rangle \\ & + \frac{1}{V} \int dV\, [1 - u_\theta(\mathbf{r})](\mathbf{f} \cdot \nabla) \int dV'\, \boldsymbol{\lambda}(\mathbf{r}') \cdot [\nabla' G(\mathbf{r}, \mathbf{r}') \times \nabla' \phi_0^{(e)}(\mathbf{r}')] \\ & + \langle (\boldsymbol{\lambda}, \nabla \phi_0^{(e)}, \mathbf{f}) \rangle \end{aligned} \tag{A.15}$$

where we have introduced the notation $(\mathbf{a}, \mathbf{b}, \mathbf{c}) \equiv \mathbf{a} \cdot (\mathbf{b} \times \mathbf{c})$ for the triple scalar product of three vectors. In the second term on the rhs of (A.15), the integration over $\mathbf{r}$ may be performed explicitly by noting that

$$\int dV\, \nabla G(\mathbf{r}, \mathbf{r}') = 0 \tag{A.16}$$

because $G = 0$ on the boundary, and that, due to the symmetry of G,

$$-\int dV\, u_\theta(\mathbf{r})\, \mathbf{f} \cdot \nabla G(\mathbf{r}, \mathbf{r}') = \Gamma \phi_{00}^{(f)} = \phi_0^{(f)} - \phi_{00}^{(f)} \tag{A.17}$$

where we also used (A.14). The second term on the rhs of (A.15) thus becomes

$$\frac{1}{V}\int dV\,\boldsymbol{\lambda}(\mathbf{r})\cdot[\nabla(\phi_0^{(f)}-\phi_{00}^{(f)})\times\nabla\phi_0^{(e)}]$$

$$=-\langle(\boldsymbol{\lambda},\nabla\phi_0^{(e)},\mathbf{f})\rangle-\langle(\boldsymbol{\lambda},\nabla\phi_0^{(e)},\nabla\phi_0^{(f)})\rangle \tag{A.18}$$

The first term on the rhs, which was obtained by noting that $\nabla\phi_{00}^{(f)}=-\mathbf{f}$, clearly cancels the last term of (A.15). Putting all this together with the definitions of $\ddot{\boldsymbol{\sigma}}_e$ and $\boldsymbol{\lambda}_e$ [see (2.3)] and separating the orders H^0 and H^1, we finally get

$$\mathbf{e}\cdot\ddot{\boldsymbol{\sigma}}_e\cdot\mathbf{f}=\langle\sigma(-\nabla\phi_0^{(e)}\cdot\mathbf{f})\rangle \tag{A.19}$$

$$(\boldsymbol{\lambda}_e,\mathbf{e},\mathbf{f})=\langle(\boldsymbol{\lambda},\nabla\phi_0^{(e)},\nabla\phi_0^{(f)})\rangle \tag{A.20}$$

These expressions may be further transformed by noting that

$$\begin{aligned}
&\langle(-\nabla\phi_0^{(e)}\cdot\mathbf{f})\rangle=\mathbf{e}\cdot\mathbf{f}\\
&\langle(\nabla\phi_0^{(e)}\times\nabla\phi_0^{(f)})\rangle=\frac{1}{V}\int dV(\nabla\phi_0^{(e)}\times\nabla\phi_0^{(f)})\\
&\qquad=\frac{1}{V}\oint(d\mathbf{A}\times\phi_0^{(e)}\nabla\phi_0^{(f)})=\frac{1}{V}\oint(d\mathbf{A}\times\phi_{00}^{(e)}\nabla\phi_0^{(f)})\\
&\qquad=\langle(-\mathbf{e}\times\nabla\phi_0^{(f)})\rangle=(\mathbf{e}\times\mathbf{f})
\end{aligned} \tag{A.21}$$

and by writing

$$\begin{aligned}
\sigma(\mathbf{r})&=\sigma_0+\sum_{i=1}^{n}(\sigma_i-\sigma_0)\,\theta_i(\mathbf{r})\\
\boldsymbol{\lambda}(\mathbf{r})&=\boldsymbol{\lambda}_0+\sum_{i=1}^{n}(\boldsymbol{\lambda}_i-\boldsymbol{\lambda}_0)\,\theta_i(\mathbf{r})
\end{aligned} \tag{A.22}$$

When these are used in (A.19) and (A.20), we get

$$\mathbf{e}\cdot\ddot{\boldsymbol{\sigma}}_e\cdot\mathbf{f}-\sigma_0(\mathbf{e}\cdot\mathbf{f})=\sum_{i=1}^{n}(\sigma_i-\sigma_0)\langle\theta_i(-\mathbf{f}\cdot\nabla\phi_0^{(e)})\rangle \tag{A.23}$$

$$(\boldsymbol{\lambda}_e-\boldsymbol{\lambda}_0,\mathbf{e},\mathbf{f})=\sum_{i=1}^{n}(\boldsymbol{\lambda}_i-\boldsymbol{\lambda}_0)\cdot\langle\theta_i(\nabla\phi_0^{(e)}\times\nabla\phi_0^{(f)})\rangle \tag{A.24}$$

Up to this point we have made no assumptions regarding any symmetries of the microgeometry. If we assume that the microgeometry has either isotropic or cubic point symmetry, then the Ohmic conductivity

becomes a scalar tensor $(\sigma_e)_{ij} = \sigma_e \delta_{ij}$ while the Hall conductivity vector becomes proportional to $\mathbf{H}$ for small H. In the case of a two-component composite we can then get especially simple results by choosing $\mathbf{e} = \mathbf{e}_x$, $\mathbf{f} = \mathbf{e}_y$, $\mathbf{H} \| \mathbf{e}_z$:

$$\frac{\sigma_e - \sigma_0}{\sigma_1 - \sigma_0} = \left\langle \theta_1 \frac{\partial \phi_0^{(x)}}{\partial x} \right\rangle \tag{A.25}$$

$$\frac{\lambda_e - \lambda_0}{\lambda_1 - \lambda_0} = \langle \theta_1 (\nabla \phi_0^{(x)} \times \nabla \phi_0^{(y)})_z \rangle \tag{A.26}$$

Note that the rhs in both equations depends, apart from the microgeometry, only on the ratio of Ohmic conductivities σ_1/σ_0.

APPENDIX B. DISCRETE NETWORK MODELS FOR THE HALL EFFECT IN A COMPOSITE MEDIUM

The models we will consider are all cubic (square in 2D)—each bond $\mathbf{a}$ lies along one of the coordinate axes x, y, z (x, y in 2D). The voltage across it V_a, which can be either positive or negative, represents the component of $\mathbf{E}(\mathbf{r})$ along the direction of $\mathbf{a}$. The components of $\mathbf{E}(\mathbf{r})$ that are perpendicular to the direction of $\mathbf{a}$ are represented by the voltages $V_{\tilde{a}}$ on neighboring bonds $\tilde{\mathbf{a}}$ that are perpendicular to $\mathbf{a}$. The models differ in the way these voltages $V_{\tilde{a}}$ are taken into account: In the model of ref. 3, the simple arithmetic average over $V_{\tilde{a}}$ on all four nearest neighbor bonds pointing in the appropriate direction was used (see Fig. 2). In our class 2 models this average is weighted by 0 or 1/4, so that only bonds of the same type as $\mathbf{a}$ contribute (see Fig. 2). In our class 1 models each bond is part of a basic unit (either a triplet or a doublet) of identical, electrically unconnected, mutually perpendicular bonds, and the only bond $\tilde{\mathbf{a}}$ which contributes to the perpendicular field is another member of the same unit (see Fig. 1).

The current in bond $\mathbf{a}$ is given by

$$J_a = g_a V_a - \sum_{\tilde{a} \in a} \lambda_{a\tilde{a}} V_{\tilde{a}}(\mathbf{e}_H, \tilde{\mathbf{a}}, \mathbf{a}) \tag{B.1}$$

where the precise meaning of the summation symbol depends on the model under consideration. The vector $\mathbf{e}_H$ is a unit vector in the direction of $\mathbf{H}$, and the triple scalar product ensures that a Hall current can only be produced in $\mathbf{a}$ by $\tilde{\mathbf{a}}$ if $\mathbf{H}$ has a nonzero component perpendicular to both $\mathbf{a}$ and $\tilde{\mathbf{a}}$. With the help of the characteristic functions

$$\theta_{ia} = \begin{cases} 1 & \text{if } \mathbf{a} \text{ is a bond of type } i \\ 0 & \text{otherwise} \end{cases} \tag{B.2}$$

we can write

$$g_a = \sum_{i=0}^{n} g_i \theta_{ia} = g_0 \left[1 - \sum_{i=0}^{n} (1 - g_i/g_0)\, \theta_{ia} \right] \equiv g_0 (1 - u_{\theta a}) \tag{B.3}$$

Kirchhoff's current conservation equations then become

$$0 = \sum_{a \in i} J_a + \sum_{a \in i} g_0 (1 - u_{\theta a})\, V_a - \sum_{a \in i} \sum_{\tilde{a} \in a} \lambda_{a\tilde{a}} V_{\tilde{a}}(\mathbf{e}_H, \tilde{\mathbf{a}}, \mathbf{a}) \tag{B.4}$$

where the first summation is over all the bonds $\mathbf{a} \equiv (ij)$ that meet at the lattice site i, and $V_a \equiv V_i - V_j$. The boundary conditions on the site potentials V_i are taken to be

$$V_i = V_{00i}^{(e)} \equiv \mathbf{r}_i \cdot \mathbf{e} \tag{B.5}$$

where $\mathbf{e}$ is a unit vector and $\mathbf{r}_i$ is the position vector at the site i. The development now proceeds in complete analogy with that of Appendix A for the continuum case (see also ref. 7): Green's tensor $\gamma_i^j\ (= \gamma_j^i)$ is defined by

$$\begin{gathered} \sum_{(ij) \in i} (1 - u_{\theta ij})(\gamma_j^l - \gamma_i^l) = -\delta_{il} \\ \gamma_i^l = 0 \text{ for } i \text{ on the surface} \end{gathered} \tag{B.6}$$

and using it, (B.4) can be transformed into

$$V_i = V_{0i} + \frac{1}{g_0} \sum_l \gamma_i^l \sum_{(lm) \in l} \sum_{\tilde{a} \in (lm)} \lambda_{lm,\tilde{a}} V_{\tilde{a}}(\mathbf{e}_H, \tilde{\mathbf{a}}, (\boldsymbol{lm})) \tag{B.7}$$

where V_{0i} is the solution of (B.4) for $\lambda_{a\tilde{a}} \equiv 0$. From this we can get the following equation for $V_a \equiv V_{ij} \equiv V_i - V_j$,

$$V_a = V_{0a} - \frac{1}{g_0} \sum_b \Gamma_{ab} \sum_{\tilde{b} \in b} \lambda_{b\tilde{b}} V_{\tilde{b}}(\mathbf{e}_H, \mathbf{b}, \tilde{\mathbf{b}}) \tag{B.8}$$

where

$$\Gamma_{ab} \equiv \Gamma_{(ij)(lm)} \equiv \gamma_i^l - \gamma_j^l - \gamma_i^m + \gamma_j^m \tag{B.9}$$

is the discrete analogue of the double gradient of the Green's function $\nabla\nabla' G(\mathbf{r}, \mathbf{r}')$. In order to get (B.8), we subtracted the equation for V_j from that for V_i and then switched the names of the dummy indices l, m, noting that $(\mathbf{m}\boldsymbol{l}) = -(\boldsymbol{lm})$. We again define γ_{0i}^j as γ_i^j for the homogeneous network,

i.e., when $u_{\theta a}=0$, and similarly Γ_{0ab}. The linear operators Γ and Γ_0 are defined by

$$\begin{aligned}(\Gamma V)_a &\equiv \sum_b \Gamma_{ab} u_{\theta b} V_b \\ (\Gamma_0 V)_a &\equiv \sum_b \Gamma_{0ab} u_{\theta b} V_b\end{aligned} \tag{B.10}$$

and are easily shown to have the same properties as the corresponding operators of Appendix A:

$$V_{0a}^{(e)} = V_{00a}^{(e)} + \sum_b \Gamma_{0ab} u_{\theta b} V_{0b}^{(e)} \tag{B.11}$$

or symbolically, in analogy with (A.11)–(A.14),

$$\begin{aligned}V_0^{(e)} &= V_{00}^{(e)} + \Gamma_0 V_0^{(e)} \\ \Gamma &= \Gamma_0 + \Gamma_0 \Gamma \\ V_0^{(e)} &= \frac{1}{1-\Gamma_0} V_{00}^{(e)} \\ \Gamma &= \frac{1}{1-\Gamma_0} \Gamma_0 \\ V_0^{(e)} &= (1+\Gamma) V_{00}^{(e)}\end{aligned} \tag{B.12}$$

The bulk effective uniform individual bond conductances g_e, λ_e are now defined and calculated by considering the individual bond current and voltage averaged over all bonds of the network:

$$\begin{aligned}\langle \mathbf{f} \cdot \mathbf{J}^{(e)} \rangle &\equiv \frac{1}{N} \sum_a \mathbf{J}_a^{(e)} (\mathbf{f} \cdot \mathbf{a}) \\ &\equiv \mathbf{e} \cdot \ddot{\mathbf{g}}_e \cdot \mathbf{f} - \lambda_e (\mathbf{e}_H, \mathbf{e}, \mathbf{f})\end{aligned} \tag{B.13}$$

Performing manipulations similar to those of Appendix A, we finally get

$$\begin{aligned}\mathbf{e} \cdot \ddot{\mathbf{g}}_e \cdot \mathbf{f} &= \frac{1}{N} \sum_a g_a V_{0a}^{(e)} (\mathbf{f} \cdot \mathbf{a}) \\ (\lambda_e, \mathbf{e}, \mathbf{f}) &= \frac{1}{N} \sum_a \sum_{\tilde{a} \in a} \lambda_{a\tilde{a}} V_{0\tilde{a}}^{(e)} V_{0a}^{(f)} (\mathbf{e}_H, \tilde{\mathbf{a}}, \mathbf{a})\end{aligned} \tag{B.14}$$

Usually we will choose $\mathbf{e}$, $\mathbf{f}$, and $\mathbf{e}_H$ to lie along the coordinate axes.

As in the continuum case, we can eliminate the summation over bonds belonging to one of the components, which can then be thought of as the

host medium g_0, $\lambda_{a\tilde{a}}^{(0)}$. In the case of a two-component medium with isotropic or cubic point symmetry we are thus led to the results

$$\frac{g_e - g_0}{g_1 - g_0} = \frac{1}{N} \sum_{a \in g_1} V_{0a}^{(x)} \mathbf{a} \cdot \boldsymbol{e}_x \tag{B.15}$$

$$\frac{\lambda_e - \lambda_0}{\lambda_1 - \lambda_0} = \frac{1}{N} \sum_{a, \tilde{a} \in g_1} \sum_{\tilde{a} \in a} V_{0a}^{(x)} V_{0\tilde{a}}^{(y)} (\mathbf{e}_z, \mathbf{a}, \tilde{\mathbf{a}}) \tag{B.16}$$

where we have taken $\mathbf{H} \| \mathbf{e}_z$ and therefore $\lambda_{a\tilde{a}}^{(i)} = \lambda_i$ if $\mathbf{a}$ and $\tilde{\mathbf{a}}$ are perpendicular adjacent bonds in the x, y plane, while $\lambda_{a\tilde{a}}^{(i)} = 0$ otherwise. The sums are restricted to bonds of type 1. In the case of the class 2 models, the rhs of (B.16) should be multiplied by an additional factor of 1/4.

APPENDIX C. THE DUALITY TRANSFORMATION IN 2D

In a two-dimensional composite made of isotropic components and lying in the x, y plane, with $\mathbf{H} \| \mathbf{e}_z$, the duality transformation consists of rotating both $\mathbf{E}(\mathbf{r})$ and $\mathbf{J}(\mathbf{r})$ by 90° in that plane. They then become, respectively, $\mathbf{J}'(\mathbf{r})$ and $\mathbf{E}'(\mathbf{r})$, which are the correct (current and electric) fields for a new problem in which the conductivity tensor is $\ddot{\boldsymbol{\sigma}}'(\mathbf{r}) = 1/\ddot{\boldsymbol{\sigma}}(\mathbf{r})$, with

$$\ddot{\boldsymbol{\sigma}} \equiv \begin{pmatrix} \sigma & \lambda \\ -\lambda & \sigma \end{pmatrix} \tag{C.1}$$

(Note that throughout this Appendix the conductivity and resistivity tensors include an antisymmetric part which represents the Hall effect.) This is shown by the following equations:

$$\begin{aligned}
\mathbf{J}'(\mathbf{r}) &\equiv \mathbf{e}_z \times \mathbf{E}(\mathbf{r}) = \begin{pmatrix} 0 & 1 \\ -1 & 0 \end{pmatrix} \mathbf{E}(\mathbf{r}) \\
\mathbf{E}'(\mathbf{r}) &\equiv \mathbf{e}_z \times \mathbf{J}(\mathbf{r}) = \begin{pmatrix} 0 & 1 \\ -1 & 0 \end{pmatrix} \mathbf{J}(\mathbf{r}) \\
\mathbf{J}'(\mathbf{r}) &= \mathbf{e}_z \times \frac{1}{\ddot{\boldsymbol{\sigma}}(\mathbf{r})} \boldsymbol{J}(\mathbf{r}) \\
&= \begin{pmatrix} 0 & 1 \\ -1 & 0 \end{pmatrix} \begin{pmatrix} \sigma(\mathbf{r}) & \lambda(\mathbf{r}) \\ -\lambda(\mathbf{r}) & \sigma(r) \end{pmatrix}^{-1} \begin{pmatrix} 0 & -1 \\ 1 & 0 \end{pmatrix} \mathbf{E}'(\mathbf{r}) \\
&= \frac{1}{\ddot{\boldsymbol{\sigma}}(\mathbf{r})} \mathbf{E}'(\mathbf{r}) \\
\nabla \cdot \mathbf{J}' &= \nabla \cdot (\mathbf{e}_z \times \mathbf{E}) = -\mathbf{e}_z \cdot (\nabla \times \mathbf{E}) = 0 \\
\nabla \times \mathbf{E}' &= \nabla \times (\mathbf{e}_z \times \mathbf{J}) = \mathbf{e}_z (\nabla \cdot \mathbf{J}) = 0
\end{aligned} \tag{C.2}$$

The only tricky point is that the new fields $\mathbf{E}'$ and $\mathbf{J}'$ may satisfy a different type of boundary condition as compared to $\mathbf{E}$ and $\mathbf{J}$. This causes no problem if the system is homogeneous on the average,[24] or if the boundary conditions are chosen appropriately.[7] If the composite is macroscopically isotropic or cubic in its point symmetry, and if the bulk effective conductivity tensor

$$\ddot{\boldsymbol{\sigma}}_e(\ddot{\boldsymbol{\sigma}}) \equiv \begin{pmatrix} \sigma_e & \lambda_e \\ -\lambda_e & \sigma_e \end{pmatrix} \tag{C.3}$$

is defined by the relation between the volume averages of $\mathbf{J}$ and $\mathbf{E}$,

$$\langle \mathbf{J} \rangle \equiv \ddot{\boldsymbol{\sigma}}_e \langle \mathbf{E} \rangle \tag{C.4}$$

then we clearly get

$$\langle \mathbf{J}' \rangle \equiv \ddot{\boldsymbol{\sigma}}'_e \langle \mathbf{E}' \rangle = \ddot{\boldsymbol{\sigma}}_e (1/\ddot{\boldsymbol{\sigma}}) \langle \mathbf{E}' \rangle \tag{C.5}$$

We can also write

$$\langle \mathbf{J}' \rangle = \begin{pmatrix} 0 & 1 \\ -1 & 0 \end{pmatrix} \langle \mathbf{E} \rangle = \begin{pmatrix} 0 & 1 \\ -1 & 0 \end{pmatrix} \frac{1}{\ddot{\boldsymbol{\sigma}}_e(\ddot{\boldsymbol{\sigma}})} \begin{pmatrix} 0 & -1 \\ 1 & 0 \end{pmatrix} \langle \mathbf{E}' \rangle$$

$$= \frac{1}{\ddot{\boldsymbol{\sigma}}_e(\ddot{\boldsymbol{\sigma}})} \langle \mathbf{E}' \rangle \tag{C.6}$$

and hence

$$\ddot{\boldsymbol{\sigma}}'_e \equiv \ddot{\boldsymbol{\sigma}}_e (1/\ddot{\boldsymbol{\sigma}}) = 1/\ddot{\boldsymbol{\sigma}}_e(\ddot{\boldsymbol{\sigma}}) \tag{C.7}$$

This exact result, which holds for arbitrary values of H, was first shown by Mendelson,[24] and was recently generalized by Milton.[25]

Specializing to the case of a 2D, two-component composite in a weak perpendicular magnetic field, we get

$$\sigma'_i = \frac{1}{\sigma_i} \quad \text{and} \quad \lambda'_i = \frac{\lambda_i}{\sigma_i^2} \quad \text{for} \quad i = 0,\ 1,\ e \tag{C.8}$$

$$\frac{\lambda_e - \lambda_0}{\lambda_1 - \lambda_0} = X\left(\frac{\sigma_1}{\sigma_0}\right) \equiv X \tag{C.9}$$

$$\frac{\lambda'_e - \lambda'_0}{\lambda'_1 - \lambda'_0} = X\left(\frac{\sigma'_1}{\sigma'_0}\right) \equiv X\left(\frac{\sigma_0}{\sigma_1}\right) \equiv X' \tag{C.10}$$

Substituting (C.8) into (C.10), and eliminating λ_e between (C.9) and (C.10), we get the following equation:

$$(\lambda_1 - \lambda_0)\left(\frac{X'}{\sigma_1^2} - \frac{X}{\sigma_e^2}\right) = \lambda_0\left(\frac{1}{\sigma_e^2} - \frac{1}{\sigma_0^2} + \frac{X'}{\sigma_1^2} - \frac{X}{\sigma_e^2}\right) \tag{C.11}$$

which must be satisfied for arbitrary values of λ_0, λ_1. Therefore the coefficients of λ_0 and of $\lambda_1 - \lambda_0$ must both vanish, and we get

$$X' = \frac{\sigma_1^2}{\sigma_e^2} \frac{\sigma_e^2 - \sigma_0^2}{\sigma_1^2 - \sigma_0^2}$$
$$X = \frac{\sigma_e^2}{\sigma_1^2} X' = \frac{\sigma_e^2 - \sigma_0^2}{\sigma_1^2 - \sigma_0^2} \tag{C.12}$$

which is the same as (2.9).

In order to apply considerations such as these directly to the discrete network models, one has to rotate the bonds together with the currents and voltages. When this is done, a class 1 network transforms into itself, but a class 2 network usually transforms into a different network, especially if it is a random network. We shall see that this difference is also reflected in the applicability of the duality transformation.

The rotated quantities J'_a, V'_a are defined as follows:

$$J'_a \equiv V_a, \qquad V'_a \equiv J_a \tag{C.13}$$

where the subscript a in the rotated quantities referes to the rotated bond **a**. When the bonds form a square network, it is easy to see that the rotated quantities have the necessary properties: Kirchhoff's current conservation equations for the J'_a flowing into a site follow from the fact that the sum of V_a around any elementary square vanishes. Similarly, the sum of V'_a around any elementary square vanishes due to current conservation of the J_a flowing into the node at its center. The next step is to try to express J'_a in terms of V'_a in a way that is reminiscent of (C.2). In order to do that, we must try to invert (B.1) into such a form, i.e.,

$$V_a = r_a J_a + \sum_{\tilde{a} \in a} R_{a\tilde{a}} J_{\tilde{a}}(\mathbf{e}_H, \tilde{\mathbf{a}}, \mathbf{a}) \tag{C.14}$$

Substituting (B.1) into this equation, we get

$$V_a = r_a g_a V_a - \sum_{\tilde{a} \in a} (r_a \lambda_{a\tilde{a}} - R_{a\tilde{a}} g_{\tilde{a}}) V_{\tilde{a}}(\mathbf{e}_H, \tilde{\mathbf{a}}, \mathbf{a})$$
$$- \sum_{\tilde{a} \in a} \sum_{a' \in \tilde{a}} R_{a\tilde{a}} \lambda_{\tilde{a}a'} V_{a'}(\mathbf{e}_H, \tilde{\mathbf{a}}, \mathbf{a})(\mathbf{e}_H, \mathbf{a}', \tilde{\mathbf{a}}) \tag{C.15}$$

Since this should be an identity, we must have

$$R_{a\tilde{a}} = \frac{r_a}{g_{\tilde{a}}} \lambda_{a\tilde{a}} \tag{C.16}$$

$$\sum_{\substack{\tilde{a} \in a \\ \tilde{a} \in a'}} R_{a\tilde{a}} \lambda_{\tilde{a}a'} = A_a \delta_{aa'} \tag{C.17}$$

where A_a remains to be determined, and where the summation is over bonds $\tilde{a}$ in a given direction, and $\mathbf{a} \| \mathbf{a}'$. Substituting from (C.16) into (C.17), we get

$$\sum_{\substack{\tilde{a} \in a \\ \tilde{a} \in a'}} \frac{r_a}{g_{\tilde{a}}} \lambda_{a\tilde{a}} \lambda_{\tilde{a}a'} = A_a \delta_{aa'} \tag{C.18}$$

There is no way that this can be satisfied for class 2 models, or for the model of ref. 3. On the other hand, it is automatically satisfied for the class 1 models, where the summation is only over one bond. In that case, since all the bonds in one unit are identical, we find

$$A_a = \frac{r_a}{g_a} \lambda_{a\tilde{a}}^2$$

$$1 = r_a g_a + \frac{r_a}{g_a} \lambda_{a\tilde{a}}^2$$

so that

$$\begin{aligned} r_a &= \frac{g_a}{g_a^2 + \lambda_{a\tilde{a}}^2} \\ R_{a\tilde{a}} &= \frac{\lambda_{a\tilde{a}}}{g_a^2 + \lambda_{a\tilde{a}}^2} \end{aligned} \tag{C.20}$$

This is clearly analogous to (C.2), and consequently we recover the exact result of (C.7) for class 1 models of any size or composition. By contrast, in the case of the class 2 models we can only hope to recover the result of (C.7) in the continuum limit, i.e., when the network is very large and the randomness is correlated over distances that are large compared to the lattice parameter. Nevertheless, we now proceeded to show that in the low-field case we can do better.

If we only need to keep terms of order H^0 and H^1, we can drop the last term in (C.15). In that case, the equation becomes an identity when

$$\begin{aligned} r_a &= 1/g_a \\ R_{a\tilde{a}} &= \lambda_{a\tilde{a}}/g_a g_{\tilde{a}} \end{aligned} \tag{C.21}$$

which is sufficient to reproduce the form of (C.2) in the low-field case. Consequently, the low-field limit of (C.7) is reproduced exactly for class 2 networks of any size or composition, including especially the result (C.12) [or (2.9)] for two-component networks.

ACKNOWLEDGMENTS

This research was supported in part by the U.S.–Israel Binational Science Foundation under grant 354/85, by NSF grant DMR 84-14257, and by the Israel National Center for Absorption in Science.

REFERENCES

1. H. J. Juretschke, R. Landauer and J. A. Swanson, *J. Appl. Phys.* **27**:838 (1956).
2. M. H. Cohen and J. Jortner, *Phys. Rev. Lett.* **30**:696 (1973).
3. I. Webman, J. Jortner, and M. H. Cohen, *Phys. Rev. B* **15**:1936 (1977).
4. J. P. Straley, *J. Phys. C* **13**:L773 (1980).
5. J. P. Straley, *J. Phys. C* **13**:4335 (1980).
6. D. J. Bergman and D. Stroud, *Phys. Rev. B* **32**:6097 (1985).
7. D. J. Bergman, in *Percolation Structures and Processes*, G. Deutscher, R. Zallen, and J. Adler, eds. (Adam Hilger, 1983), p. 297.
8. D. J. Bergman, Y. Kantor, D. Stroud, and I. Webman, *Phys. Rev. Lett.* **50**:1512 (1983).
9. U. Dai, A. Palevski, and G. Deutscher, *Phys. Rev. B* **36**:790 (1987).
10. M. Rohde and H. Micklitz, *Phys. Rev. B* **36**:7289 (1987).
11. B. Derrida and J. Vannimenus, *J. Phys. A* **15**:L557 (1982).
12. E. Duering and D. J. Bergman, in preparation.
13. C. D. Mitescu, M. Allain, E. Guyon, and J. Clerc, *J. Phys. A* **15**:2523 (1982).
14. P. N. Sen, J. N. Roberts, and B. I. Halperin, *Phys. Rev. B* **32**:3306 (1985).
15. C. J. Lobb and D. J. Frank, *J. Phys. C* **12**:L827 (1979).
16. R. Fogelholm, *J. Phys. C* **13**:L571 (1980).
17. B. Derrida, D. Stauffer, H. J. Herrmann, and J. Vannimenus, *J. Phys. Lett.* (Paris) **44**:L701 (1983).
18. J. Hoshen and R. Kopelman, *Phys. Rev. B* **14**:3438 (1976).
19. H. J. Herrmann, D. C. Hong, and H. E. Stanley, *J. Phys. A* **17**:L261 (1984).
20. S. Wilke, *Phys. Lett. A* **96**:344 (1983).
21. D. W. Heermann and D. Stauffer, *Z. Phys. B* **44**:339 (1981).
22. S. Marianer and D. J. Bergman, *Phys. Rev. B* **39**:11900 (1989).
23. D. J. Bergman, *Physica A* **157**:72–88 (1988).
24. K. S. Mendelson, *J. Appl. Phys.* **46**:4740 (1975).
25. G. Milton, *Phys. Rev. B* **38**:11296–11303 (1988).